Master's thesis

NTNU
Norwegian University of Science and Technology
Faculty of Medicine and Health Sciences
Kavli Institute for Systems Neuroscience

Monika Irene Overdevest

Regional changes in parvalbumin and calbindin expression in fear memory circuits of the developing mouse brain

Master's thesis in Neuroscience
Supervisor: Ingvild E. Bjerke
Co-supervisor: Menno P. Witter and Trygve B. Leergaard
November 2022

NTNU
Norwegian University of
Science and Technology

UNIVERSITY OF OSLO

Monika Irene Overdevest

Regional changes in parvalbumin and calbindin expression in fear memory circuits of the developing mouse brain

Master's thesis in Neuroscience
Supervisor: Ingvild E. Bjerke
Co-supervisor: Menno P. Witter and Trygve B. Leergaard
November 2022

Norwegian University of Science and Technology
Faculty of Medicine and Health Sciences
Kavli Institute for Systems Neuroscience

NTNU
Norwegian University of
Science and Technology

Sammendrag

Uttrykt i nevroner og vidt distribuert i den voksne musehjernen finner vi kalsiumbindende proteiner. Gjennom utvikling bidrar kalsiumbindende proteiner som parvalbumin og calbindin til modningen av nevrale nettverk som ligger til grunn for en rekke funksjoner, inkludert fryktminneprosesser. Tidligere forskningsfunn konkluderte med at et redusert nivå av disse bindende proteinene kan føre til nevrodegenerative sykdommer og videre være involvert i nevroutviklingsforstyrrelser som angst. Ettersom de fleste studier kun fokuserer på en eller få hjerneregioner er informasjon om antall og tetthetsfordeling av disse kalsiumbindende proteinene i den utviklende musehjernen fragmentert. For å gi en mer omfattende oversikt over mengden og fordeling av kalsiumbindende proteiner i musehjernen, har vi laget en betydelig samling av mer enn 2500 mikroskopiske bilder. Disse bildene viser utviklingsmønsteret til parvalbumin og calbindin positive nevroner, fra musehjerner i alderen 9, 14, 21 og 35 dager. Dette prosjektet gir en analyse fokusert på nettverket som er assosiert med fryktminne, bestående av prelimbisk område, infralimbisk område og basolateral amygdala. Resultatene viser økt nivå av parvalbumin positive nevroner gjennom utvikling mens calbindin nivåer synker. Den største forskjellen ble sett i basolateral amygdala, som indikerer at disse kalsiumbindende proteinene spiller en avgjørende rolle i fryktminneprosesser under utvikling. All data innhentet i dette prosjektet deles offentlig gjennom forskningsinfrastrukturen EBRAINS, som gjør det mulig for forskere å undersøke videre regionale endringer i hjernens arkitektur gjennom utvikling.

Abstract

Calcium-binding proteins expressed in neurons are widely distributed across the adult mouse brain. Through development, calcium-binding proteins such as parvalbumin and calbindin contribute to the maturation of neural networks underlying a range of functions such as fear memory processes. Previous research findings concluded that a decreased level of these binding proteins may result in neurodegeneration and further be involved in neurodevelopmental disorders such as anxiety. Information on the number and density distribution of these binding proteins in the developing mice brain are fragmented, as most studies focus only on one or few brain regions. To provide a more comprehensive overview of the amount and spatial distribution of calcium-binding proteins in the mouse brain, we have created a comprehensive collection of more than 2500 microscopic images. These images illustrate the developmental pattern of parvalbumin and calbindin positive neurons, sampled from the brains of mice aged 9, 14, 21, and 35 days. To demonstrate how this material can be used, the present project provides an analysis focused on areas associated with fear memory networks including prelimbic area, infralimbic area and basolateral amygdala. Our results indicate that parvalbumin levels increase through development while calbindin levels decrease. The largest difference was seen in basolateral amygdala indicating that these binding proteins play a crucial role in fear memory processes during development. All data resulting from this project are publicly shared through the EBRAINS research infrastructure, allowing researchers to further investigate regional changes in brain architecture through development across the entire brain.

Acknowledgments

The present master project was carried out in the Neural Systems Laboratory, Institute of Basic Medical Sciences, under the supervision of Dr. Ingvild E. Bjerke and Prof. Trygve B. Leergaard, with additional supervision from Prof. Menno P. Witter, Kavli Institute for Systems Neuroscience, NTNU. The project was in part supported by the European Union Horizon 2020 Framework Program for Research and Innovation (945539 Human Brain Project SGA3 to TBL), The Research Council of Norway (Norges forskningsråd, 269774 INCF Norwegian Node to TBL and MPW), and UNIFOR Frimed (2021 and 2022 to TBL). Histological sections were digitized using the NORBRAIN slidescanning service at the Institute of Basic Medical Sciences.

This endeavor would not have been possible without supervision of Dr. Ingvild E. Bjerke, for her endless patience, feedback, and all the help through the entire process not least keeping never-ending hours spent in the lab fun.

I would like to thank my fellow labpartner Olga Rogulina, for collaborating on collecting and processing data for this project. Grateful for our stimulating discussions and hours of testing our patience with slow software.

I could not have undertaken this journey without Grazyna Babinska and Hong Qu for teaching me everything I know about lab safety and the processing of countless slides, respectively.

Special thanks to Menno P. Witter and Trygve B. Leergaard for your feedback and support on this project.

Lastly, I would like to acknowledge my family, especially my parents and grandparents. Their support and belief in me have kept me highly motivated during this journey. And not least, my friends for always listening to my rollercoaster ride through this project and for endless discussions for inspiration.

Table of Contents

List of Figures

List of Tables

List of Abbrevations

ABC	Avidin-biotin complex
BLA	Basolateral amygdala
BSA	Bovine serum albumin
CB	Calbindin
CBP	Calcium-binding protein
DAB	3.3-diaminobenzidine
H_2O_2	Hydrogen peroxide
ILA	Infralimbic area
NaPi	Sodium phosphate buffer
NDS	Normal donkey serum
PBS	Phosphate buffered saline
PFA	Paraformaldehyde
PLA	Prelimbic area
PV	Parvalbumin
TRX	Triton X-100

1 Introduction

Through infancy and adolescence, the brain undergoes major reorganization. To study neuropathological changes occurring in brain disorders that manifest during adolescence, detailed knowledge on structural changes occurring across the brain during normal development is essential. However, analyses of how specific cell types evolve brain wide throughout development are lacking. In particular, there is a need for brain wide overview of cells expressing calcium-binding proteins, which are abundant in the brain and of importance for a range of brain function. Knowledge about the normal development of these neurons may also propose needed insight into structural changes occurring across the brain during abnormal development where mental and neurodevelopmental disorders including anxiety disorders, Alzheimer's disease, autism (Trutzer et al., 2019), and schizophrenia (Reynolds et al., 2004; Sakai et al., 2008) are sensitive to manifest. Taken together, there is a need to advance our understanding of how specific cell types evolve across brain regions through different stages of development with brain wide data. This project will contribute to producing such data, while also providing a focused analysis on anatomical areas supporting fear memory circuitry.

1.1 Development

The anatomical formation of the nervous system takes place during early development. During the embryonic stage, the neural tube develops into the spinal cord (Brust et al., 2015) and five subsections, which will later form the brain, specifically, the myelencephalon, metencephalon, mesencephalon, diencephalon, and telencephalon. In the course of the neuronal tissue maturation phase, the brain circuits are highly plastic (Brust et al., 2015). In mice, a major part of neurogenesis is completed (Takahashi et al., 1996) by the time of birth. However, at this stage, molecular cues continue to guide the growth and migration of synapses, cells, and axons (Dimmock & Lawlor, 2017) to wire brain networks. Rearrangement of neurons in an experience-dependent process is also vital for the resulting functional networks seen in adults. Indeed, the development of neurons and the network they form correlates with the type of input they receive, and diverse sets of conditions are required for the formation of functional synapses (Tyzio et al., 1999). In other words, external and internal influential factors continue to rearrange the neural networks throughout development. Normal development involves dynamic changes in the number and distribution of various cell types contained in each area of the brain, and different regions of the brain develop at different rates (Zheng et al., 2007). Neurons expressing calcium-binding protein such as calbindin (CB) and parvalbumin (PV) are of special interest because of their ability to modulate calcium signals and contribute to the process of fear memory. Information about the quantity of neurons expressing calcium-binding protein across different brain regions through development is required to recognize how regions mature and how these neurons establish their functional roles in behaviors and processes.

1.2 Fear memories are consolidated and stored by specific anatomical regions

Fear memory is an extensively studied form of memory. Circuits involved in the formation of fear include mainly the hippocampus, basolateral amygdala (BLA), and lateral amygdala, in addition to the prelimbic area (PLA), infralimbic area (ILA), central amygdala and the dentate gyrus (Izquierdo et al., 2016). Models of fear learning have

been useful for the examination of memory consolidation as a whole. Areas related to fear memory (Schulreich et al., 2020) analyzed in this project include the PLA, ILA, and BLA (Fig. 1). The PLA is located in the medial prefrontal cortex, dorsal to the ILA (Mukherjee & Caroni, 2018). The BLA is found ventral to hippocampus and lateral to the midbrain. Both the PLA and ILA have been found to possess largely distinct projections connecting to BLA (Riaz et al., 2019). Stress is found to enhance fear learning, which is a process closely connected to and mediated by the BLA (Izquierdo et al., 2016) as well as fear response and the consolidation of fear memories. Long-term consolidation of fear memory depends on the activity-dependent induction of intracellular signaling pathways that encourage processes such as protein synthesis (Young & Thomas, 2014). Furthermore, research has brought to light a functional dichotomy between the PLA and ILA (Riaz et al., 2019). While the PLA promotes the expression of context-dependent fear, contrary, ILA is associated with the inhibition of these behaviors. Interestingly Sharpe and Killcross (2015) uncovered when working with rodents that PLA and ILA were involved in different functions of fear response when exposed to shock stimuli in different contexts. Supporting the findings of Riaz et al (2019), Sharpe and Killcross concluded that the PLA allowed for higher-order cues to adjust both responding towards and learning about, different cues. Inactivation of PLA disrupted the encoding and expression of context-dependent association. Recent studies have taken advantage of in vitro observations of plasticity in these areas in the study of memory processes, and suggest that regulation of networks in specific areas could be used in treatment. Moreover, the extinction of fear memory processes would include in the mentioned structures, a reverse of the information flow and could be used in therapy of disorders resulting from fear memory processes (Izquierdo et al., 2016). In other words, a decline in fear response

towards stimuli that are connected to fear processes could be a result from regulating connection between networks.

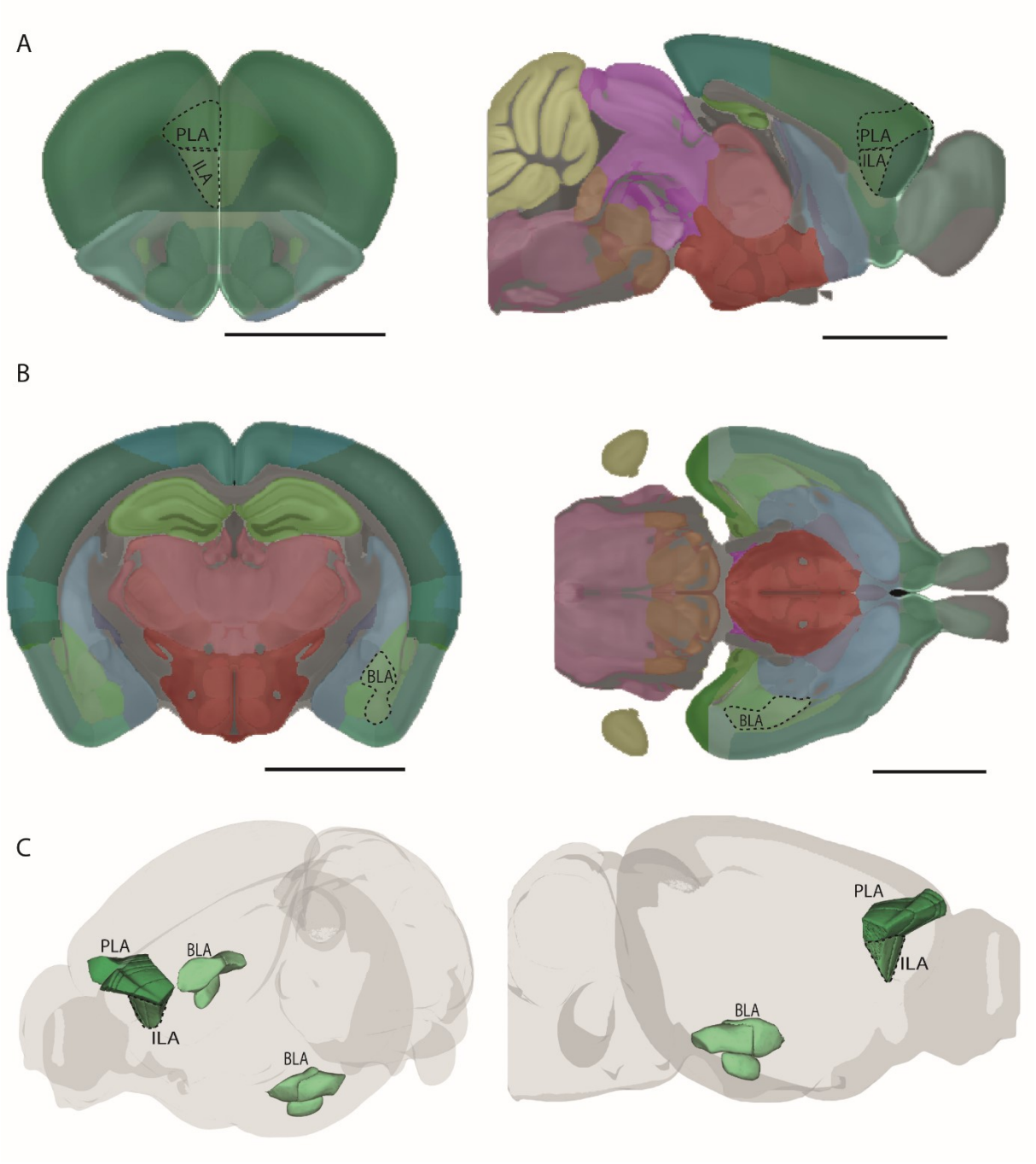

Figure 1 Regions of interest. Overview of areas analyzed in this project. (A) A coronal and midsagittal view of Prelimbic area (PLA), and Infralimbic area (ILA). (B) Basolateral amygdala (BLA) seen from a coronal and horizontal view. (C) A 3D view of the three regions of interest showing their relative positions in the mouse brain. Scale bars are 3mm.

1.3 Calcium-binding proteins

Calcium is a mineral that has several important functions in cellular processes. Calcium concentrations in the nervous system are tightly regulated by calcium-binding protein (CBP), chains of amino acids that bind calcium ions. There are several types of CBP involved in specific functions throughout the nervous system. These proteins are essential for several functions within cells including homeostasis (Nelson & Chazin,

1998), acting as a buffer for incoming calcium ions (Elíes et al., 2020), to learning, and memory processes (Evans & Blackwell, 2015.; Molinari, Battini, et al., 1996). There is no doubt that CBP acts as the ultimate multitasker.

1.3.1 Role and function in the brain

A great number of CBP is expressed in the brain (Schwaller, 2020) regulating brain networks involved in memory processes, spatial navigation, and social interactions (Harris et al., 2016). CBP modulate the temporal and spatial dynamics of the calcium signaling pathway by binding to Ca^{2+} ions. Temporary increases in intracellular calcium concentrations are found to play a critical role in the regulation of neurotransmitter release, synaptic plasticity, neural excitability (Berridge, 1998), and homeostasis. However, toxic rise in intracellular calcium is an important cue in several neurodegenerative processes (Fairless et al., 2019). The decline of CBP within a cell leads to toxic accumulation of Ca^{2+} (Ruden et al., 2021). This results in the collapse of the mitochondrial membrane potential, electron transport, and further may lead to activation of the apoptotic pathway, in other words, programmed cell death. Thus, CBP add an important defense mechanism through their ability to buffer incoming calcium before it reaches toxic intracellular levels and are able to maintain homeostasis. Calcium binding proteins are involved in several processes including homeostasis and wiring of different brain systems (Hof et al., 1999).

Importantly, the construction of memory is dependent on CBP in the process of memory formation and elimination. Calcium ions are essential in storing new memories and skills by activating the postsynaptic signaling pathways for both the weakening and strengthening of synapses (Evans & Blackwell, 2015). Evans et al., (2015) argue that these opposing processes are dependent on amplitude, duration, and location to determine which molecules preferentially bind calcium and influence memory formation and elimination. The study of calcium signaling is adding knowledge on the mechanism of various processes. Fairless et al., (2019) suggest that CBP may be a crucial key to survival, understanding neurodevelopmental disorders (Elíes et al., 2020), and serving as beneficial markers of various neuronal subpopulations for developmental and anatomical studies.

1.3.2 Cell types

Among the many CBP in the brain, parvalbumin (PV) and calbindin (CB) are notably striking in the complementarity of their distribution and their abundance (Bjerke et al., 2021). PV and CB are found in various subpopulations of neurons regulating brain networks (Harris et al., 2016; C Miao et al., 2017). During development, PV and CB are fluently expressed, supporting several aspects of brain establishment, maturation of neuronal networks, and construction of different brain systems (Hof et al., 1999). Altered levels of neurons expressing PV and CB contribute to the establishment of motor (Medina et al., 2014), and sensory systems (Desgent et al., 2010; Schmidt-Kastner et al., 1992). Moreover, PV and CB are being explored as having a key role in several processes and functions (Elíes et al., 2020) from homeostasis to synaptic plasticity. Neurons expressing CB generally outnumber PV positive neurons in the adult murine models in the three areas of interest for the current thesis (Bjerke et al., 2021).

1.4 Parvalbumin

PV belongs to the EF-hand family, which in detail can be described as a helix structural domain that binds calcium ions (Ca^{2+}). PV contains three domains, binding three Ca^{2+} ions, acting as a cytosolic calcium buffer. In the nervous system PV positive

neurons show fast-spiking electrophysiological phenotypes (Markram et al., 2004), meaning high-frequency firing rate with short-duration action potentials. Neurons expressing PV play an important role in oscillatory network activities due to their properties (Sohal et al., 2009), these properties include input from large ensembles of principal cells and providing feedback resulting in synchronization. Interestingly, PV is specifically expressed in a subgroup of GABAergic interneurons and are highly vulnerable to stressors which have been linked to neuronal damage, brain aging, and neurodegenerative diseases (Ahn et al., 2017; Ruden et al., 2021). According to Fairless et al (2019) PV positive neurons are more liable to degeneration.

1.4.1 Cell distribution

PV is found in neuronal populations such as amacrine cells, cerebellar purkinje neurons, cortical basket cells, interneurons, corticostriatal projection neurons, hippocampal interneurons, retinal ganglion cells (Fairless et al., 2019), and some stellate cells (Gattoni & Bernocchi, 2019). Mostly, PV is present in interneurons throughout the nervous system and expressed in areas related to spatial navigation and sensorimotor processing (Bjerke et al., 2021).

1.4.2 Function and role

In cells, PV acts as a calcium buffer, protecting the cell from toxic levels of calcium in mitochondria and promoting ATP production (Ruden et al., 2021). PV positive interneurons are excellent at converting excitatory input to an inhibitory output rapidly (Kawaguchi et al., 1987; Lübke et al., 1997), they are suited to control target cell's output (Wouterlood et al., 1995) and are reliably activated during high-frequency stimulation because they do not accommodate (Jones & Bühl, 1993; McCormick et al., 1985). These interneurons express fast responses and effective inhibition of surrounding principal neurons (Hu et al., 2014). Inhibitory neurons are characterized by a narrow spike waveform, and they are fast-spiking which results in short recovery periods, a feature that provides fast synaptic responses (Rudy et al., 2011). Interestingly, PV interneurons have been found to have larger dendritic trees and thicker dendrites than other interneurons which gives PV interneurons high metabolic activity by structure (Ruden et al., 2021). Notably, these interneuron's connections are predominantly perisomatic and are understood to play a role to create and maintain gamma oscillations. Ruden et al (2021) highlights that gamma oscillations help improve working memory, reduce amyloid plaque formation, and premature cell death linked to the restoration of voltage-gated sodium channels. The synchronized network ensured by PV interneurons leads to an increase in gamma oscillations during stimulation. Interestingly, gamma oscillations in humans are associated with elevated working memory load (Gonzalez-Burgos et al., 2015).

Individual PV interneurons connect to almost every local pyramidal neuron which help facilitate synchronized networks (Ferguson & Gao, 2018; Packer & Yuste, 2011) by receiving input from these interneurons. From early stages of life through adolescence these networks are associated with plasticity and function in both feedback and feedforward inhibition which regulates sensory responses such as learning and memory processes. Courtin et al (2014) found, in mice, when presenting a fear associated tone, that activity in PV interneurons is strongly reduced during fear association. This fear associated tone produced a massive activation of excitatory neurons in the prefrontal cortex that drives fear expression (Courtin et al., 2014). In other words, PV interneurons are deactivated during fear memory formation. Furthermore, PV play an important role in memory processes and the deletion of PV results in consequences for this function

(Ruden et al., 2021). Therapeutic strategies should be explored to prevent their role in several brain disorders which are tied to dysfunctional interneurons (Ruden et al., 2021).

1.5 Calbindin

Another member of the EF-hand family is CB, consisting of six domains binding to four Ca^{2+} molecules, and acts as a cytosolic calcium buffer. In other words, CB stabilize the concentration of free calcium ions within cells and are expressed in populations of both inhibitory and excitatory neurons (Jinno & Kosaka, 2006; Szabadics et al., 2010). Moreover, in the nervous system CB positive neurons show burst-spiking electrophysiological phenotypes (Ahn et al., 2017; Markram et al., 2004) explained as an alternation between high-frequency spikes and quiescence.

1.5.1 Cell distribution

CB is localized within dendrites, cell body, and axons of specific populations of neurons such as cerebellar purkinje neurons, cortical nonpyramidal neurons, granule cells of the dentate gyrus, hippocampal pyramidal neurons, and retinal ganglion cells (Fairless et al., 2019). CB positive neurons are found in various forebrain areas involved in memory processes, and dominate in regions reflecting behavioral states (Bjerke et al., 2021). Neurons expressing CB are found to be abundant in the areas of interest for this thesis (i.e the PLA, ILA, and BLA), and of interest to consider their role in memory processes (Molinari, Batjini, et al., 1996), more specific fear. Furthermore, according to Kemppainen and Pitkanen (2000), CB positive neurons seem to be distributed differently in the various nuclei of amygdala and among those, are found in the BLA. In BLA, CB positive neurons seems to form basket-like arrangement around CB negative projection neuron somata (Berdel & Morys, 2000; Legaz et al., 2005; Muller et al., 2003). This points to an interesting role of CB in the mentioned area because of the particular powerful control axo-somatic synapses possess over target neurons compared to distal dendritic or spine connections during early postnatal life through maturation.

1.5.2 Function and role

Research have pointed to an interesting theory that cells containing CB are protected from degeneration caused by conditions that increase intracellular calcium concentration (McMahon et al., 1998). In other words, by binding to free floating calcium ions the CB help preventing cell degeneration. Reports have shown that during aging a slow decrease in CB expression occurs which seems to be a simple downregulation of the expressing protein and not directly neuronal decrease (Fairless et al., 2019). Further, Fairless et al (2019) proposed that CB positive areas are associated with resistance, while a decrease in expression within a cell may suggest cellular death as a result. These findings support that CB have a neuroprotective role and delay the onset of necrosis and apoptosis after excitotoxic stimulation. CB is found to protect the cell from damage and decreased expression of CB is associated with cell dysfunction. In short, concentration of CB is essential for normal cell function. According to Berdel and Morys (2000), CB is closely associated with the maturation of BLA, PLA and ILA.

1.6 Dysfunction in parvalbumin and calbindin neurons

In addition to their essential role in normal cell function, PV and CB positive neurons may serve as a key link in the process of neurodegeneration, neurodevelopmental disease, and memory processes. Notably, fear memory processes are a natural biological mechanism needed in situations that requires survival behavior. The absence or excess of CBP could lead to dysfunction of memory processes and other

abnormalities such as anxiety disorders, Alzheimer's disease, schizophrenia, autism, epilepsy (Fairless et al., 2019). Thus, the maintenance of calcium homeostasis within neurons is essential for normal cell function involved in several mechanisms. A rise in intracellular calcium levels may result in the onset of apoptosis due to toxic environment damaging the mitochondria (Ruden et al., 2021). CBP help the regulation of homeostasis, synaptic plasticity, and memory processes (Berridge, 1998). Influx of calcium into the postsynaptic neuron helps shape the event of memory processes. Harris et al (2016) created mice with reduced levels of CB and concluded that reduced levels of CB in neurons disrupted behavior connected to fear and anxiety due to the network these neurons interact with, more specific connection between PLA, ILA and BLA. Furthermore, Nieves et al., (2020) found altered expression of parvalbumin in areas related to fear learning in mice exposed to limited bedding. Moreover, when young mice gets maltreated and/or neglected as a result from limited nesting materials during development, a delay in physical development and increased counts of PV positive neurons were found. More specific, an increase of neurons expressing PV were found in BLA and changes in PLA and ILA to BLA connectivity during early development. Remarkably, these mice failed to exhibit threat associated fear behavior during the period of elevated expression of PV (Nieves et al., 2020) however, this learned fear re-emerged at later stages of development**.** These findings suggest that calcium binding proteins are underlying essential pathways for memory processes and play a key role in normal cell function. Yet, the mechanisms underlying the dysfunction of specific neuronal subpopulations are not fully understood. Increased insight of these processes will be of great interest of effective neuroprotective strategies for the future (Fairless et al., 2019).

1.7 Summary of the state of the field

There is a steady flow of research concerning the structure and function of the brain. As we have seen, CBP is crucial for maintaining normal cell functions and neurons expressing PV and CB are heavily involved in the regulation of fear memory processes. Thus, PV and CB may play a crucial role in various neurodevelopmental disorders (Hu et al., 2014) including anxiety disorders. In the future, neurons expressing PV and CB may become imperative therapeutic targets. Research has pointed to large numbers of PV expression in PLA found in adult murine models, while expression of PV positive neurons found in BLA and ILA is sparse, in contrast, neurons expressing CB are abundant in BLA and ILA (Bjerke et al., 2021). Pointing to different roles PV and CB may play in areas they are expressed. However, most research focuses on the adult models thus knowledge about the developmental trajectories of brain regions involved in fear memory processes remains vague.

1.8 Aim

The purpose of this project is to study the development of two specific CBP types that have recently been mapped across the adult murine brain (Bjerke et al., 2020). Specifically, to investigate neurons expressing the two CBP, PV and CB. The focus of this thesis is to examine the regional changes in PV and CB expression in fear memory circuits of the developing mouse brain, more specific PLA, ILA, and BLA. However, PV and CB are essential for several functions in a various range of cell types. Their location is important to understand their role and functions including neuronal populations regulating brain networks involved in memory processes, spatial navigation, and social interactions (Harris et al., 2016; Chao Miao et al., 2017). Gathering information on the amount of these neurons across brain regions is necessary to understand the maturation of brain regions. Thus, while this thesis focuses on expression patterns in three regions

of interest, the data acquisition will be performed brain-wide to support investigations of other brain regions in the future.

2 Methods

2.1 Animals

In total, 30 C57BL/6 mice of postnatal day P9, P14, P21, and P35 were used for this research (n = 6-8 mice in each age group). Further, 3-4 mice in each age group were analyzed specific for this project. Animals from the youngest age groups (P9 and P14 were bred locally, while animals from the P21 and P35 groups were purchased from Janvier Labs). All brains were used for both calbindin (CB) and parvalbumin (PV) staining. Necessary approvals for animal research were obtained from the Norwegian Food Safety Authority (FOTS approval no. 12717 and 28114) and animals were treated in in accordance with the European Union and International legislation for the use of animal subjects.

2.2 Perfusion

Surgically anesthetized mice were sacrificed by transcardial perfusion with a buffered paraformaldehyde solution (see appendix A). Animals were perfused in groups of six at separate times depending on their age and when they were bred. The goal of this procedure was to keep the morphology intact and preserve the brain tissue against decay. Perfusion of the animals was conducted in the morning between 8 am and 12 noon. Adjustment in equipment used and handling strategies was done for the younger groups. The adjustment in equipment was crucial to get usable perfused P9 and P14 brains when extracted because the young age groups were more delicate.

2.2.1 Fixative and perfusion buffer

Ice-cold 2% dextran and room temperature 4% PFA in NaPi pH 7,4 was used. The perfusion apparatus was filled with fresh solutions before each perfusion.

2.2.2 Apparatus and anesthesia

Tubes from the perfusion apparatus were flushed with fixative solution to prevent air bubbles entering during the perfusion and then filled with ice-cold buffer right before each use.

Individual weight were noted to calculate the anesthesia dose. Mice were deeply anaesthetized using a ZRF cocktail, 0.1ml per 10g were calculated and administered as dose to effect. The animal was then injected intraperitoneally and left under surveillance for 5-10 minutes to make sure the mice was fully anaesthetized. To check for this, a tweezer was used to pinch the animal's toes. The animal was prepared for surgery when there was no reaction from the toe pinch.

2.2.3 Perfusion surgery

The mouse was mounted to the working area using four syringe needles, one for each paw. Then a tweezer and scissor were used to cut a V shaped area from the pelvic area and upwards until reaching the left and right armpit of the mouse. The excess skin and ribs was folded over and fastened with another syringe needle. The diaphragm and the pericardium attachments was cut for free flow of returning blood and perfusion. The perfusion needle was inserted into the left ventricle.

2.2.4 Perfusion

As soon as the perfusion needle was inserted into left ventricle the apparatus was set to start. Using a setting between 12 and 22 for speed, dependent on the size and age of the animal.

2.2.5 Dissection

The head was separated from the body with a scissor and a midline incision was made from the upper part of the neck to expose the skull. Pointing the scissor upwards at all times to prevent damage to the perfused brain, a tweezer and sharp scissors were used combined for a careful incision and removal of the skull and tissue surround to access the brain and extract it in a whole piece. In younger animals, generally tissue and skull are softer and noticeably smaller because of development.

2.2.6 Post-fixation and storage

Immediately after extraction, the brain was placed into a container with 4% PFA. After 24 hours, the solution was changed to 0.1% PFA.

2.3 Brain sectioning

Before sectioning, the brains were cryoprotected by immersion in sucrose solutions of 10%, 20% and 30%, each time until the brain sank to the bottom. First there was a small incision made on the right hemisphere of the brain to indicate later the brain's orientation. The whole brain was photographed next to a ruler for size information. The brains where then placed on a flat surface and cut coronally with a razor blade into two blocks (fig. 2). Further, each block was mounted and frozen to the stage of the freezing microtome at -40 Celsius and sectioned at 40 micrometer at -20 Celsius. Some tissue was lost from each block due to sectioning quality from the last pieces. An interval between 100-200 micrometers were considered lost from each block. To avoid losing the same part of the brain each time, the coronal cut of the brain into two blocks were made at different places each time. Approximately 350 sections from each brain were each put into separate wells with NaPi and 0.1% PFA solution and stored for immunohistochemistry.

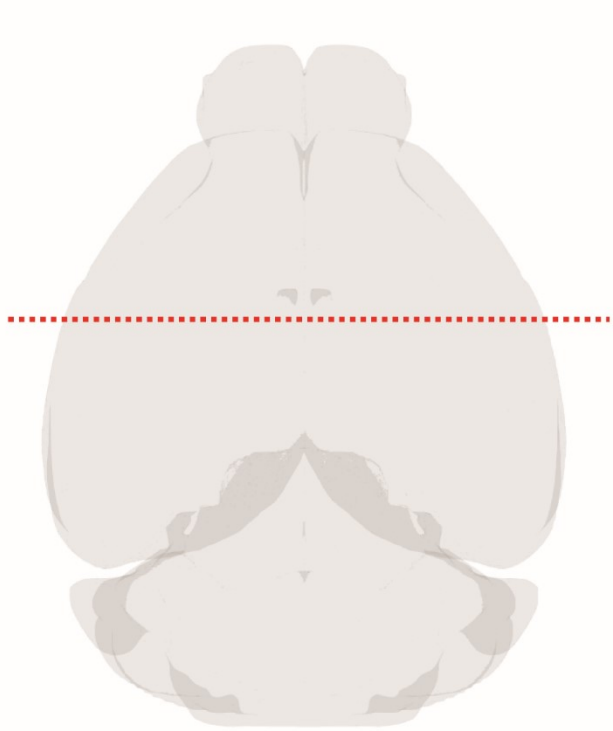

Figure 2 Orientation of cut. Here, the brain is seen from above and the red dotted line indicates a coronal cut.

2.4 Immunohistochemistry

For each brain, every 6th section was selected and made into series to be processed for CB and every 6th for PV. A negative control section was included for each brain, to ensure that omitting the primary antibody incubation would result in no specific labelling. All steps were performed at room temperature unless otherwise specified. To avoid evaporation of the liquid in the wells, parafilm was added under the lid and used for all incubations exceeding 10 minutes (see appendix B).

On the first day, sections were washed with PBS three times ten minutes then blocked in PBS with 3% H^2O^2 for five minutes. Sections were washed again with PBS three times five minutes then incubated in blocking buffer (PBS with 10% NDS, 1% BSA and 0.5% TRX) for one hour. Lastly, the sections were incubated in primary antibody over night at 4 degrees Celsius on a rotating table. A monoclonal mouse anti-calbindin (RRID:AB_10000347) was used for CB staining and a monoclonal rabbit anti-parvalbumin (RRID:AB_2631173) for PV staining, both for primary antibody incubation. These antibodies were diluted in incubation buffer (PBS with 3% NDS, 1% BSA and 0.1% TRX) at 1:5000 for CB and 1:4000 for PV.

The next day, sections were washed in PBS with 0.2% TRX three times ten minutes. Secondary antibody incubation was performed for one hour at a rotating table. Sheep anti mouse (RPN1001V, GE Healthcare) was used for CB and donkey anti rabbit (RPN1004V, GE Healthcare) used for PV. Washed again in PBS with 0.2% TRX two times ten minutes then one time for ten minutes in PBS. ABC solution was prepared in between the wash cycle 15-30 minutes before being used. This kit (pk-6100, Vector Laboratories) is an enzymatic, avidin/biotin based amplification system that produces crisp, high sensitive, specific staining that could easily be distinguished from background staining. Sections were then incubated in ABC for 30 minutes on rotating table and again washed in PBS with 0.2% TRX two times ten minutes and one time ten minutes in PBS. Under the fume hood chromogenic reaction with DAB-kit was prepared immediately before use and dependent on the staining let sit 5 minutes for CB and 2 minutes for PV. These times were decided based on previous tests. DAB kit sk-4100 produced a brown reaction in the presence of peroxidase enzyme (Vector DAB). The reaction was stopped with sterile MQ water wash two times five minutes and then washed again one time ten minutes in PBS.

After the last PBS wash, sections were mounted to gelatin coated slides, with 3-4 sections mounted per slide. Sections were transferred into a petri dish then carefully placed onto the gelatin coated glass precisely and in the correct orientation. All sections were aligned with the midline perpendicular to the long axis of the slide. The slides were air dried before being dehydrated in EtOH solution 2 min each in 70%, two times in 96%, two times in 100% and two times in xylene. Lastly, the slides with sections were coated with second glass slide using Eukitt and stored dry overnight before scanning.

2.5 Scanning and organizing of images

Gelatin coated slides were scanned using Axioscan (Zeiss) slide scanner. Then the scanned files were opened in Zen 2.6 blue edition (RRID:SCR_013672) to adjust white balance and export TIFF files. Nutil Transform Nutilv0.6.0 (RRID:SCR017183) were used to batch process files to rename, define rotation, flip, downscaling and orientation of the scanned files. Some files were edited in Adobe Photoshop (RRID:SCR_014199) to correct for mounting errors.

2.6 Registration and analysis

Once all the files were renamed and ensured to be in the correct orientation, they were spatially registered to Allen mouse brain reference atlas using the QuickNII tool (RRID:SCR_016854). This project has taken advantage of these 3D atlases to analyze the mouse brain at different stages during development. Versions of QuickNII bundled with developmental brain atlases appropriate for each age group were applied (Newmaster et al., 2020). Versions of QuickNII corresponding to the four age groups explored are specified as QuickNII_AMBA-DEV-P7/P14/P21/P28. All images were spatially registered to the age-relevant atlas. This tool allowed for manual rotation and scale to

match the anatomical landmark visible in each image. From QuickNII, JSON files were created and used in VisuAlign (RRID:SCR_017978) to non-linearly fit brain regions of interest to the correct areas in the images (fig. 3).

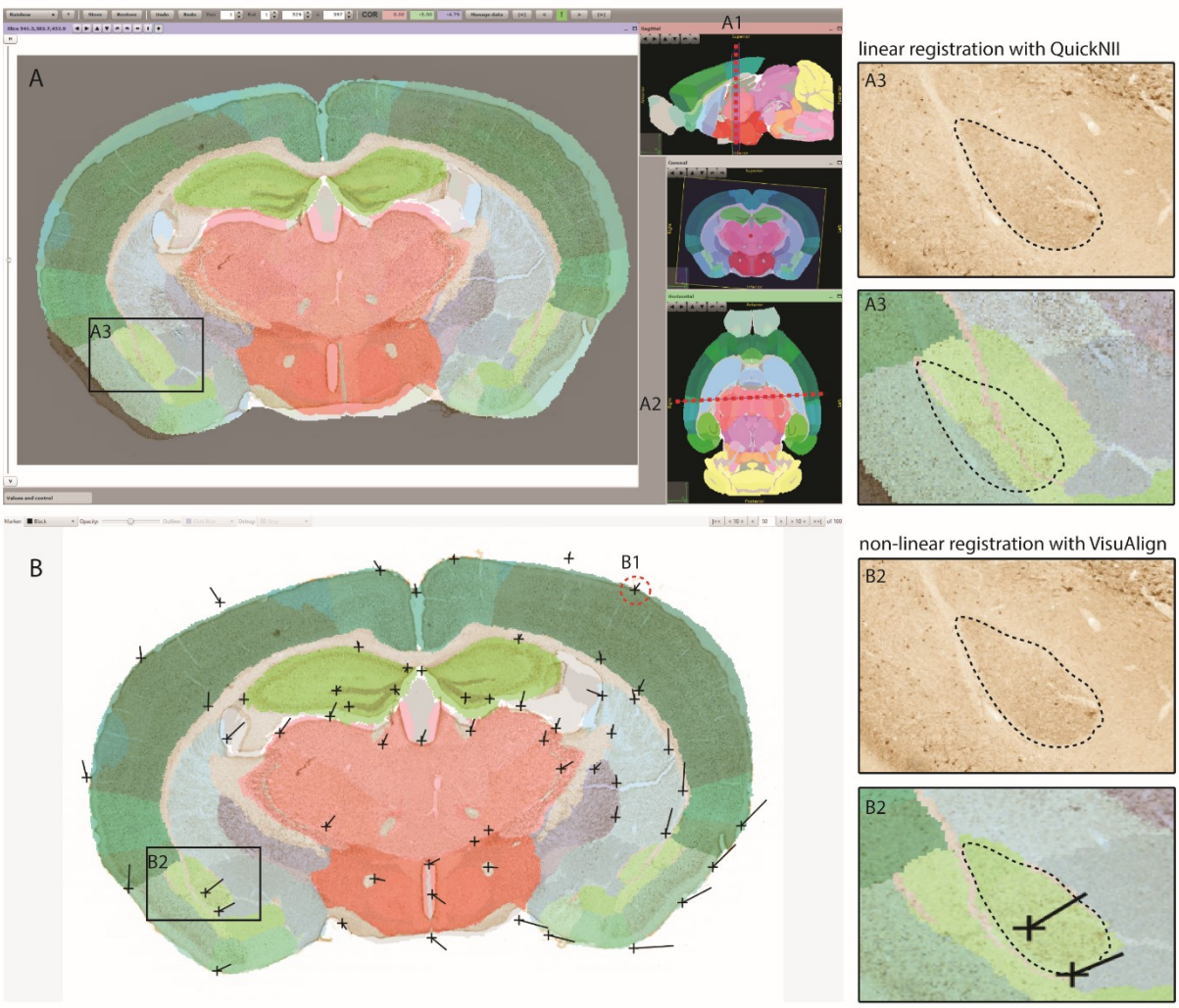

Figure 3 Registration workflow. (A) Data were anchored in QuickNII. (A1, A2) Here the atlas were cut to exactly match the section angle. The red dotted line illustrates the present image's angles. (A3) Illustrates a linear registration where the atlas overlay to fit the underlying section, limited to only be stretched and shrunk. (B) Mismatches from QuickNII were accounted for by using VisuAlign. (B1) illustrates the marks that were set to fit the atlas map and it's orientation to the images. (B2) Here the atlas overlay were non-linearly transformed to fit the section.

The 3D atlases used to compare landmarks in the current experimental images are a great aid to define brain regions. A match between anatomical landmarks in the experimental image and reference atlas are made and the relationship between experimental image and atlas are defined across the entire series of images.

Further, Ilastik (RRID:SCR_015246) were applied to all data. This machine-learning based software help distinguish cell from background. Few manual inputs of what should be considered cell and what should be background helps the program to recognize the features of interest. A live-update function were used on the training images until the match between what is cell and what is background were perfected.

Then, the software was used to batch process the rest of the images (fig. 4).

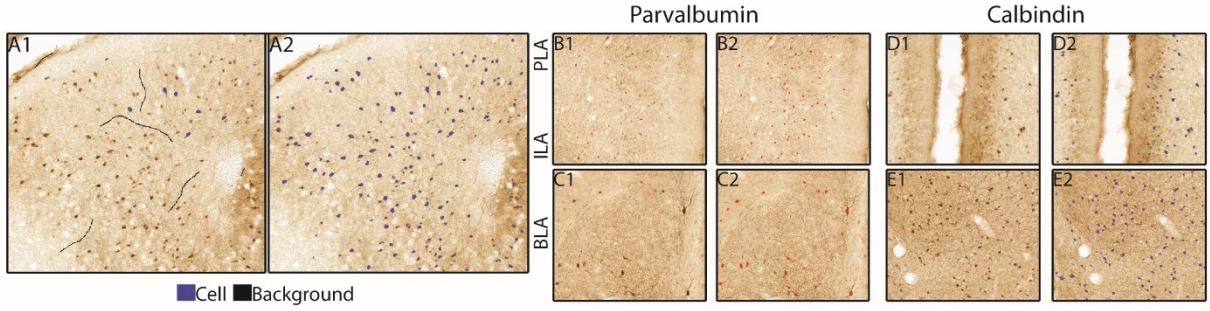

Figure 4 Image segmentation. Ilastik is a machine-learning based software and illustrated above. (A1) Shows how examples of what should be considered cell and what should be considered background are input manually. (B) The machine gradually learns to recognize the features of interest. The training was done on a representative subset of the material and then used to batch process all the images. (B1, C1, D1, E1) Areas of interest before being processed. (B2, C2, D2, E2) areas of interest after being processed.

To combine the segmented images with the results of the spatial registration, Nutil quantifier was used. This was used as a workflow to quantify cellular parameters across the whole brain to allow for visualization of color coded objects of interest in reference atlases. Settings in Nutil were set to recognize objects larger than 4 pixels as one neuron. Damaged areas were masked using Adobe Photoshop before going through Nutil quantifier. Whenever an area in a section was damaged, the average counts from the neighboring sections were used instead. Next, to find the total number and neuron density estimates for each region of interest, the process of multiplication were used to account for section sampling interval and Abercrombie's formula were used to adjust for the tendency of overestimations when extrapolating numbers. Then, the total number of neurons were divided by the volume for each region to find neuron densities per cubic millimeter.

Final analyses were done using IBM SPSS Statistics 28.0.0.0 (RRID:SCR_016479). Scatter plot charts were based on data from PV and CB positive neurons found in each area in SPSS. Descriptive statistical analysis was carried out in excel on data collected from total number of neurons and neuron density from each area of interest. Each area was examined separately.

3 Results

The data collection presented here consists of more than 2500 microscopic images showing neurons expressing parvalbumin (PV) and calbindin (CB) immunolabelling across the brains of young mice. Histological sections from young (postnatal days 9, 14, 21, and 35) mouse brains was immunostained and digitized, and images were spatially registered to 3D brain reference atlases to facilitate comparisons across age groups. A semi-automatic workflow was used to quantify changes in three brain regions related to fear memory.

In the following, qualitative observations describing the general developmental pattern for PV and CB positive neurons will first be described. Second, the quantitative data will be presented describing the total number and densities of CB and PV positive neurons from the three regions of interest, prelimbic area (PLA), infralimbic area (ILA) and basolateral amygdala (BLA). The developmental patterns of these neurons across the different age groups will be described separately for PV and CB.

3.1 Parvalbumin

3.1.1 Qualitative observations

Observations of PV-stained sections indicate that the labelling, meaning overall neurons expressing PV, is sparse and limited to few regions across the brain at early stages (P9 and P14). Interestingly, overall data shows a dense collection of PV-stained neurons in primary somatosensory area, reticular nucleus of thalamus and globus pallidus of the youngest age group and span out just few days after (from P14). Qualitatively, it appears that overall PV neuron expression reach adult like pattern between P14 and P21. However, quantitative analyses may reveal more subtle changes.

3.1.2 Quantitative analysis

The numbers and densities of parvalbumin neurons in the regions of interest for each age group, resulting from the quantitative analysis, are presented in Table 1.

Age	SubjectID	TotalPLA	TotalILA	TotalBLA	DensityPLA	DensityILA	DensityBLA
P35	m172	2454	774	1300	1680	1133	1905
	m192	3338	1064	1895	2015	2799	1876
	m532	3324	1027	1806	1871	1420	2068
	m708	1895	959	1280	1558	1566	2587
	MEAN	**2753**	**956**	**1570**	**1781**	**1729**	**2109**
	SD	**611**	**112**	**282**	**175**	**637**	**285**
P21	m127	1953	446	1131	1329	1221	1726
	m137	2085	673	1747	1621	1646	2002
	m178	2198	895	1904	1842	1999	2393
	MEAN	**2078**	**671**	**1594**	**1598**	**1622**	**2040**
	SD	**100**	**183**	**333**	**210**	**318**	**274**
P14	m104	1544	785	1048	1155	1635	1886
	m720	1641	691	1838	1049	1675	2768
	m878	759	448	1173	602	945	1596
	MEAN	**1315**	**641**	**1353**	**935**	**1418**	**2083**
	SD	**395**	**142**	**347**	**240**	**335**	**498**
P9	m274	127	102	351	109	167	445
	m431	142	40	282	145	93	317
	m518	166	83	221	114	140	319
	m693	255	232	504	300	420	493
	MEAN	**172**	**114**	**340**	**167**	**205**	**393**
	SD	**50**	**71**	**106**	**78**	**127**	**77**

Table 1 Descriptive statistics for the total number and density estimates for parvalbumin neurons in the prelimbic area, infralimbic area and basolateral amygdala. Individual values for each mouse are given, and for each age group the two rows highlighted in bold give the mean and standard deviation.

3.1.3 Prelimbic area

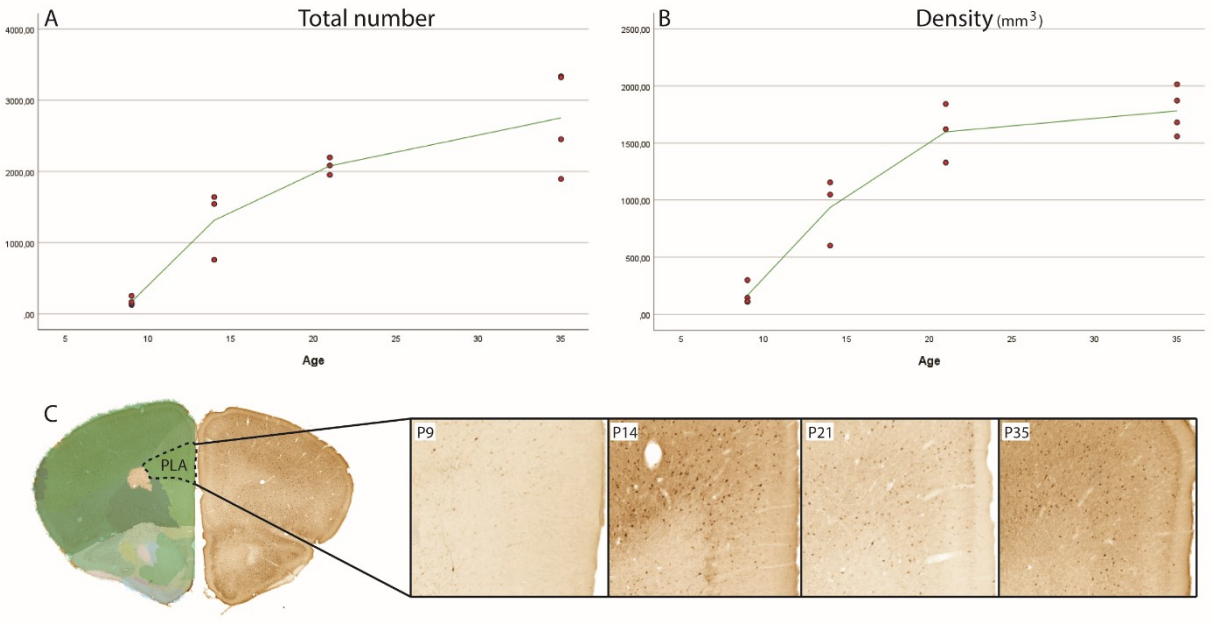

Figure 5 Parvalbumin distribution in prelimbic area. (A and B) Graphs representing total number (A) and density (mm^3) (B) of parvalbumin positive neurons found in prelimbic area across the four age groups. (C) Example images from prelimbic area in P9 through P35. Neurons expressing parvalbumin indicates a denser population and an adult-like pattern from P14.

Figure 5 illustrates the total number and density of neurons expressing PV found in PLA in the different age groups. Both the number (*mean* = 172, *SD* = 50) and density estimates (*mean* = 167 cells / mm^3, *SD* = 78) are low at P9 (n = 4). At P14 (n = 3) the number (mean = 1315, SD = 395) and density estimates (mean = 935 cells / mm^3, SD = 240) are increasing. From P21 (n = 3) the number (mean = 2078, SD = 100) and density estimates (mean = 1598 cells / mm^3, SD = 210) shows an increase. At P35 (n = 4) the number (mean = 2753, SD = 611) and density estimates (mean = 1782 cells / mm^3, SD = 175) flattens out. Thus, both the total number and density estimates indicates a rapid increase in neurons expressing PV from P9 through P14. Density has a steeper incline from P14 to P21, both total number of neurons and density seem to flatten out from P21, consistent with the qualitative observations of adult like patterns at this stage.

3.1.4 Infralimbic area

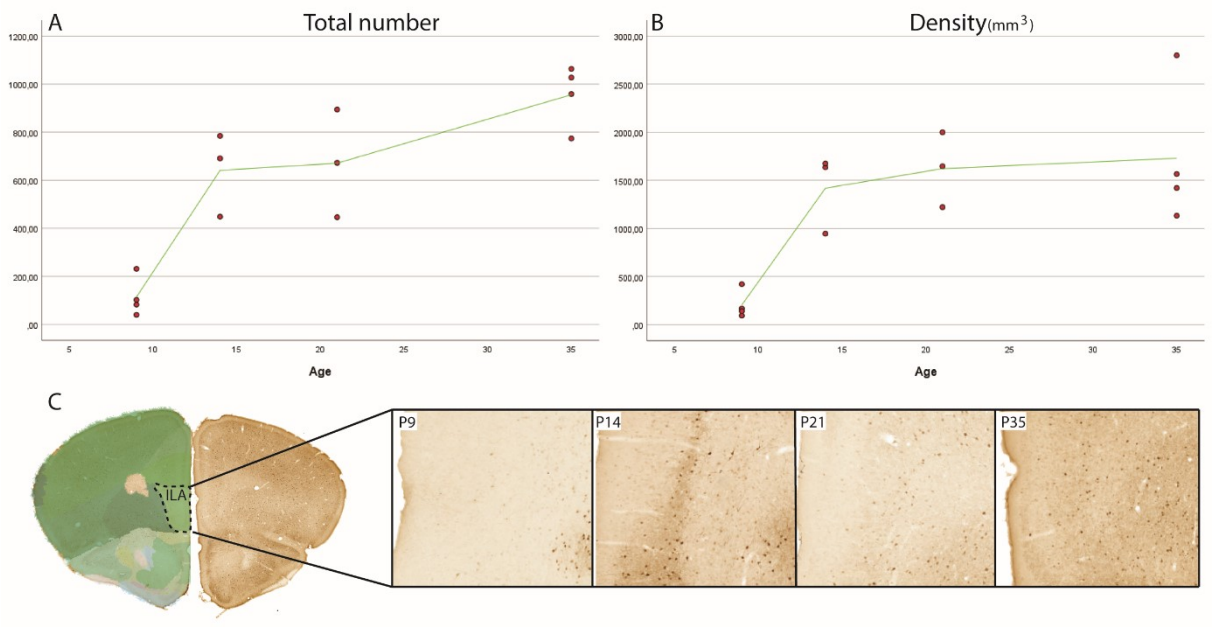

Figure 6 Parvalbumin distribution in infralimbic area. (A and B) Graph representing total number (A) and density (mm^3) (B) of parvalbumin positive neurons found in infralimbic area across the four age groups. (C) Example images from infralimbic area in P9 through P35. Showing a denser population of parvalbumin positive neurons from P14.

Figure 6 shows the total number and density of PV positive neurons found in ILA in the different age groups. Both the number (*mean* = 114, *SD* = 71) and density estimates (*mean* = 205 cells / mm^3, *SD* = 127) are low at P9 (n = 4). At P14 (n =3) the number (mean = 641, SD = 142) and density estimates (mean = 1418 cells / mm^3, SD = 335) shows a steep increase. From P21 (n = 3) the number (mean = 671, SD = 183) and density estimates (mean = 1622 cells / mm^3, SD = 318) indicates a line that flattens out. At P35 (n = 4) the number (mean = 956, SD = 112) and density estimates (mean = 1729 cells / mm^3, SD = 637) has a steeper increase in total number of neurons found compared to neuron density which has a flatter line but still increasing. Thus, both the total number and density estimates show a rapid increase in neurons expressing PV from P9 through P14. Total number have a steeper incline from P21 to P35, both total number of neurons and density seem to flatten out from P14.

3.1.5 Basolateral amygdala

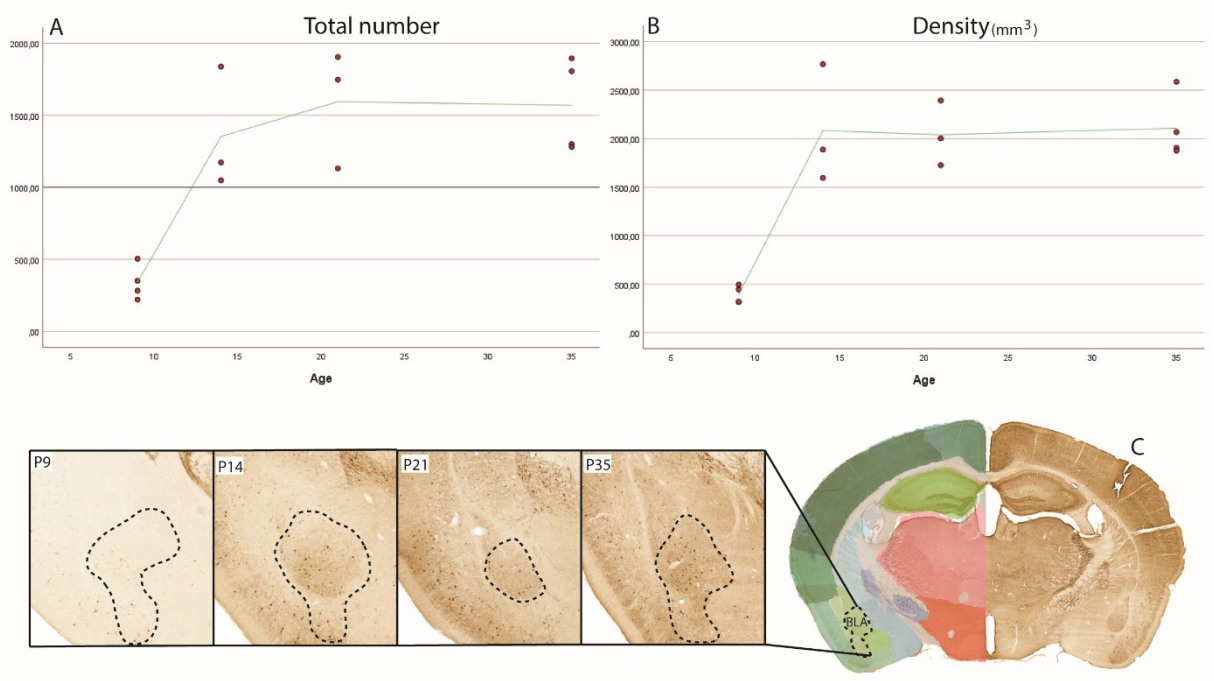

Figure 7 Parvalbumin distribution in basolateral amygdala. (A and B) Graph representing the total number (A) and density (mm^3) (B) of parvalbumin positive neurons found in basolateral amygdala across the four age groups. (C) Example images from basolateral amygdala in P9 through P35. Parvalbumin neurons are almost unnoticed in P9, showing an adult-like pattern from P14 with dense population at P35.

Figure 7 illustrates the total number and density of neurons expressing PV found in BLA in the different age groups. Both the number (*mean* = 340, *SD* = 106 and density estimates (*mean* = 393 cells / mm^3, *SD* = 77) are low at P9 (n = 4). At P14 (n = 3) the number (mean = 1353, SD = 347 and density estimates (mean = 2083 cells / mm^3, SD = 498) has a steep increase. From P21 (n = 3) the number (mean = 1594, SD = 333 and density estimates (mean = 2040 cells / mm^3, SD = 274) seems to stabilize. At P35 (n = 4) the number (mean = 1570, SD = 282 and density estimates (mean = 2109 cells / mm^3, SD = 285) flattens out. Thus, both the total number and density estimates show a rapid increase in neurons expressing PV from P9 through P14. Neuron density has a steeper incline from P9 to P14, both total number of neurons and density seem to flatten out beginning from P14, consistent with the qualitative observations of adult like patterns at this stage. High numbers of neurons expressing PV at P9 and pattern appear adult-like at P14 like in later stages.

3.2 Calbindin

3.2.1 Qualitative observations

At first glance, expression of CB-stained neurons in cortical areas at P9 is wide-spread. Interestingly, it seems like neurons expressing CB are rare in areas where PV are abundant and vice versa, until the mice reach the age of P21. The amygdala contains a large number of CB positive neurons but few PV positive neurons in all age groups analyzed. Neuron expression of CB in thalamus is limited in contrast to neuron expression of PV in young mice. Overall, expression patterns of CB appear adult-like from P21.

3.2.2 Quantitative analysis

The numbers and densities of calbindin neurons in the regions of interest for each age group, resulting from the quantitative analysis, are presented in Table 2.

Age	SubjectID	TotalPLA	TotalILA	TotalBLA	DensityPLA	DensityILA	DensityBLA
P35	m172	9591	4294	6667	5634	6998	7012
	m192	8960	3874	3757	7711	6618	7547
	m532	6180	3175	5204	3197	4179	4724
	m708	4043	2225	2449	2737	4818	4786
	MEAN	**7194**	**3392**	**4519**	**4820**	**5653**	**6017**
	SD	**2226**	**783**	**1577**	**2000**	**1184**	**1277**
P21	m127	5856	1658	6322	4650	3358	9140
	m137	6175	2805	3767	3998	5504	5340
	m178	7074	3690	7187	4139	6948	6571
	MEAN	**6368**	**2718**	**5759**	**4263**	**5270**	**7017**
	SD	**516**	**832**	**1452**	**280**	**1475**	**1583**
P14	m104	6794	2186	4044	6257	4896	9586
	m720	6046	2017	7419	4413	6693	7504
	m878	6041	2513	6416	7827	6581	9422
	MEAN	**6294**	**2239**	**5960**	**6166**	**6057**	**8837**
	SD	**354**	**206**	**1415**	**1395**	**822**	**945**
P9	m274	5156	2718	6726	4381	4882	8046
	m431	4067	2076	6235	5104	5403	9692
	m518	4022	2423	5465	4903	10125	9319
	m693	5748	2949	6725	6332	6709	9841
	MEAN	**4748**	**2542**	**6288**	**5180**	**6780**	**9225**
	SD	**734**	**327**	**515**	**715**	**2043**	**706**

Table 2 Descriptive statistics for the total number and density estimates for calbindin neurons in the prelimbic area, infralimbic area and basolateral amygdala. Individual values for each mouse are given, and for each age group the two rows highlighted in bold give the mean and standard deviation.

3.2.3 Prelimbic area

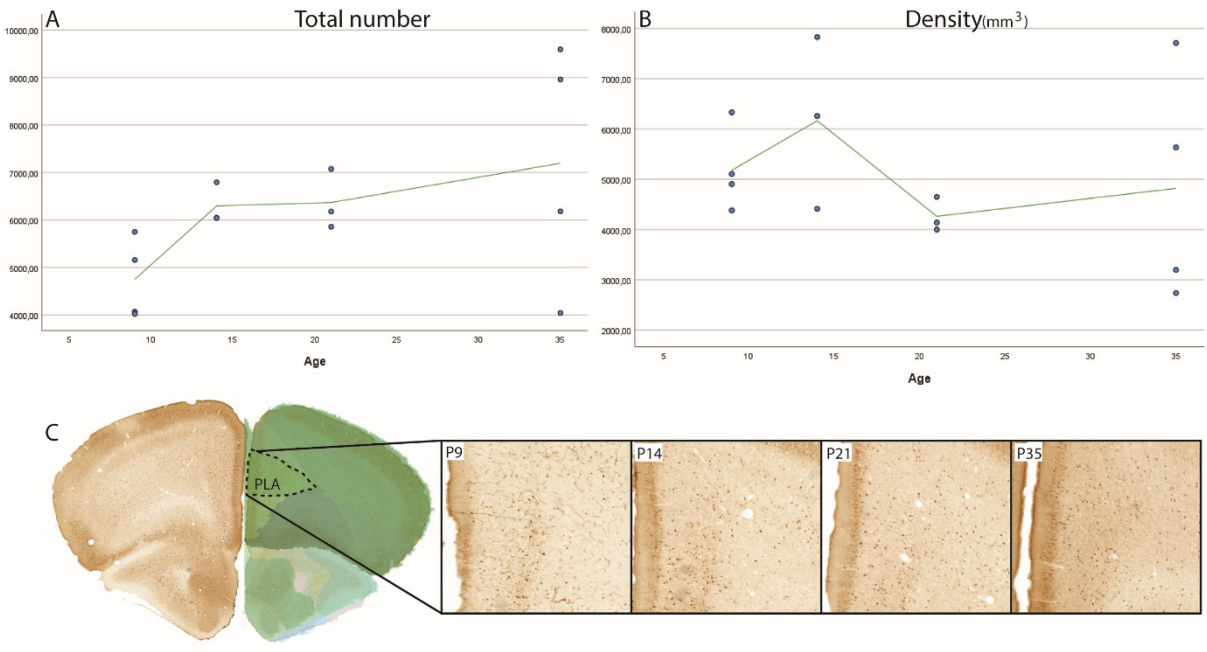

Figure 8 Calbindin distribution in prelimbic area. (A and B) Graph representing total number and density (mm^3) of calbindin positive neurons found in prelimbic area across the four age groups. (C) Example images from prelimbic area in P9 through P35. Calbindin neurons are abundant from early stage of development. Further showing a matured network in P35.

Figure 8 shows the total number and density of neurons expressing CB found in PLA in the different age groups. The total number (*mean* = 4748, *SD* = 734) is low at P9 while density estimates (*mean* = 5180 cells / mm^3, *SD* = 715) are high (n = 4). Towards P14 (n = 3) both the number (mean = 6294, SD = 354) and density estimates (mean = 6166 cells / mm^3, SD = 1395) are increasing. Density indicate a drop from P14 to P21 while number indicate an increase between each age group. From P21 (n = 3) the number (mean = 6368, SD = 516) stabilizes and density estimates (mean = 4263 cells / mm^3, SD = 280) drops. At P35 (n = 4) the number (mean = 7194, SD = 2226 and density estimates (mean = 4820 cells / mm^3, SD = 2000) shows signs of a little increase but seems to flatten out. Here the total number of neurons and density estimates appears to be similar at P9 but when total number increase the neuron density decrease by P35. Both seem to flatten out from P21, consistent with the qualitative observations of adult like patterns at this stage.

3.2.4 Infralimbic area

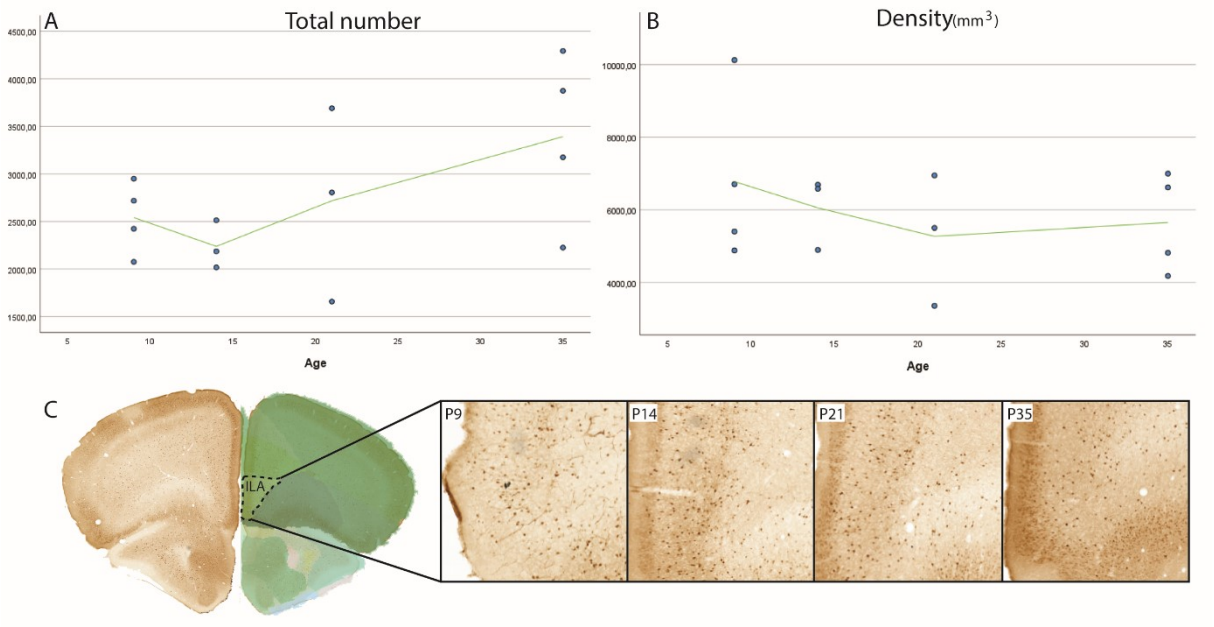

Figure 9 Calbindin distribution in Infralimbic area. (A and B) Graph representing total number and density (mm^3) of calbindin positive neurons found in infralimbic area across the four age groups. (C) Example images from infralimbic area in P9 through P35. Calbindin positive neurons are abundant from early stage of development. Further showing a matured network in P35.

Figure 9 illustrates the total number and density of CB positive neurons found in ILA in the different age groups. The number (*mean* = 2542, *SD* = 327) at P9 begins at the lower end of the y-axis while density estimates (*mean* = 6780 cells / mm^3, *SD* = 2043) are at its highest (n = 4). Towards P14 (n =3) both the number (mean = 2239, SD = 206) and density estimates (mean = 6057 cells / mm^3, SD = 822) drops slightly. The drop in density seem to last until P21 while number begins to increase again from P14. At P21 (n = 3), the number (mean = 2718, SD = 832) increases and density estimates (mean = 5270 cells / mm^3, SD = 1475) continues to drop slightly. While both the number (mean = 3392, SD = 783) and density estimates (mean = 5653 cells / mm^3, SD = 1184) increases towards P35 (n = 4), the total number of neurons displays a steeper climb.

3.2.5 Basolateral amygdala

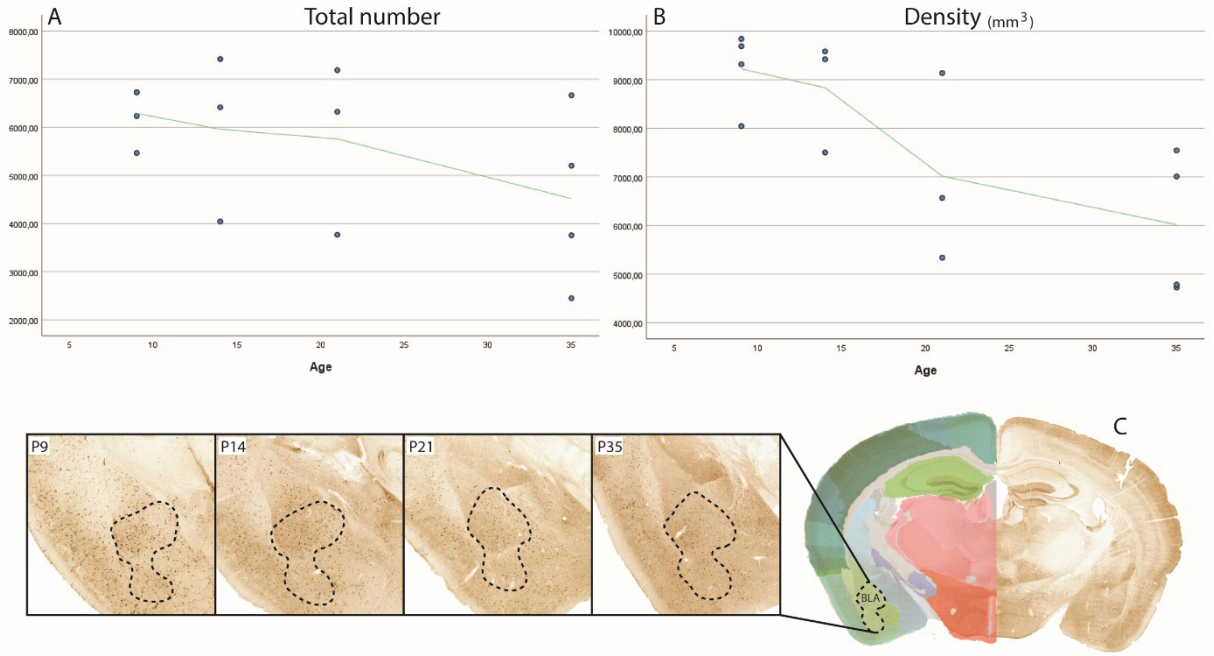

Figure 10 Calbindin distribution in basolateral amygdala. (A and B) Graph representing total number and density (mm³) of calbindin positive neurons found in basolateral amygdala across the four age groups. (C) Example images from basolateral amygdala in P9 through P35. Calbindin neurons are abundant from early stage of development. Further showing a sparse distribution of neurons expressing calbindin in P35.

Figure 10 shows the total number and density of CB positive neurons found in BLA in the different age groups. Both the number (*mean* = 6288, *SD* = 515 and density estimates (*mean* = 9225 cells / mm^3, *SD* = 706) are high at P9 (n = 4). At P14 (n = 3) the number (mean = 5960, SD = 1415 and density estimates (mean = 8837 cells / mm^3, SD = 945) shows a decrease. From P21 (n = 3) the number (mean = 5759, SD = 1452) and density estimates (mean = 7017 cells / mm^3, SD = 1583) continue to decrease while density has a steeper drop. At P35 (n = 4) the number (mean = 4519, SD = 1577) and density estimates (mean = 6017 cells / mm^3, SD = 1277) still show a decrease. Thus, both the total number of neurons and density estimates indicates a decrease of neurons expressing CB from P9 through P35. Density have a steeper decline from P9 to P21, both total number of neurons and density seem to flatten out beginning from P21, consistent with the qualitative observations of adult like patterns at this stage.

3.3 Quality

The quality of PV and CB stained sections varied between subjects and within subjects. Notably in the youngest age group where CB stained subjects had noise in form of blood vessels (fig. 11). Compared to PV stained sections taken from the same area and subject where a noticeable difference is present. This was true for all CB data in P9.

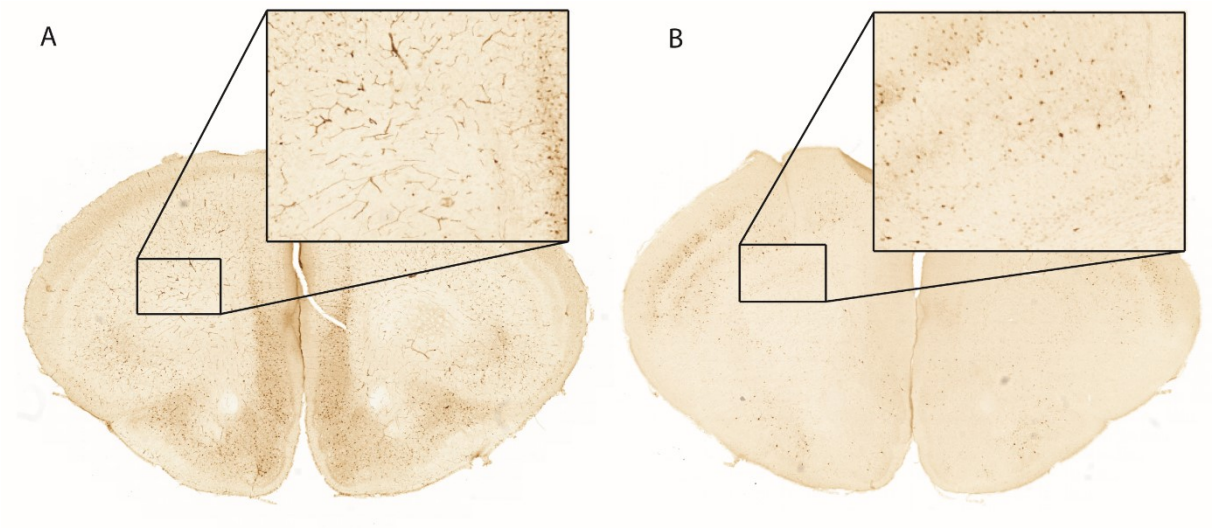

Figure 11 Data quality. (A) Noise from blood vessels in calbindin stained sections from P9. (B) Clarifies the same area and subject in parvalbumin stained section. Interestingly, the noise was mostly present in calbindin stained sections from the youngest age group.

4 Discussion

The current research project has provided quantitative data on calbindin (CB) and parvalbumin (PV) positive neurons in basolateral amygdala (BLA), prelimbic area (PLA) and infralimbic area (ILA) of the developing mouse brain. Their location is important to understand their functions and maturation of brain regions. The fluctuations in calcium-binding protein (CBP) in the specific areas are most pronounced in the early stages of development. Later expression patterns stabilize during adolescence. Interestingly, both total number of neurons expressing PV and density tended to increase in all investigated areas, whereas neurons expressing CB tended to decrease. In the following, I will first discuss the efficiency of the research methodology used for this thesis. I will go on to elaborate on the quantitative data in the areas of interest and explore the connection these changes may have to development of fear memory. Lastly, I will discuss the relevance of this research findings to human development, and how the data created here may be re-used in new analyses.

4.1 Methodological limitations

A number of factors in the methodological approach might influence results, such as the quality of perfusion, and sensitivity of the immunostaining. Sample size and lost sections are important factors to mention. Perfusion results for the brains used in this thesis were generally good, although they may differ slightly between age groups, as perfusing the very small mice of the youngest age groups presented a particular technical challenge. In addition to the quality of the perfusion itself, other factors such as stress induced, and circadian rhythm of the animal at the time being perfused may be a factor influencing results from individual brains, even though this is yet to be analyzed. Detailed notes of the perfusion parameters and results were kept and are included in Appendix C.

Sample size and variations between sexes such as different size of brain areas are other limitations relevant to consider. For this research, both male and female mice were included, but questions regarding sexual dimorphism were not possible to address because of the modest sample size. However, the total sample size of the project is larger than that used for analysis here, and with some further expansion of the material such questions could be explored in the future. Some micrometers of each brain were naturally lost during the cutting method. Although this cut was made in different places for each brain to avoid systematic loss of any brain regions, it is possible that regions in the middle of the brain are more often affected. Thus, the BLA, a region of interest in this study, might have been critically influenced by this. Which may have resulted in a lack of data on these areas even when trying to compensate for it by avoiding systematic loss.

Several limitations for resulting data were found during immunostaining, which is a technique used to identify cells expressing a protein of interest by binding the protein to an antibody resulting in a darker stain. Most anterior part of PLA was lost or damaged during immunostaining due to small pieces that were difficult to keep track of. Notably, the use of immunostaining to identify CB and PV positive neurons reveals only broad cell classes not subtypes (Bjerke et al., 2021) which the project's protocol did not allow classifications for. To elaborate, resulting data only identifies overall neurons expressing PV and CB, and did not reveal what population of neuron.

Moreover, the use of atlas registration and image analysis grant efficient quantification across the brain, but the acquisition of correct number of cells depended on the darkness of stain and pixels in each cell counted using semi-automated image

analysis. During the cutting, some cells might be split and can appear in several sections leading to over counting (Abercrombie, 1946). By the use of Abercrombie's formula these biases were corrected for. Some subsets of PV and CB positive neurons were lightly stained which during segmentation were not fully successfully extracted. Thus, there may be an underestimation of cell number and size, however, this affects all age groups equally when cell areas were calculated. It is also necessary to mention the possibility that some of the young brains stained for CB displayed staining of blood vessels in our results, probably due to sub-optimal perfusions (see fig. 11 above). Although the segmentation results were generally deemed satisfactory also for these brains, there may be a slightly higher level of false positives in the segmentation from these brains.

4.2 Developmental patterns of calbindin and parvalbumin neurons

These results show that CB positive neurons generally outnumber PV positive neurons in all areas of interest in the developing mouse brain. The most striking example of this contrast was seen in the youngest age group analyzed where PV positive neurons are sparse (<400 per mm^3) and neurons expressing CB are elevated (>5000 per mm^3) in all areas. The magnitude of this difference is reduced over time during development. In P14 and P21 the CB positive regions have relatively high numbers but shows a drop in PLA and BLA from P14 to P21. Whereas all areas (PLA, ILA, and BLA) increase in numbers of PV positive neurons. Thus, through development, neuron expression of PV increased and CB decreased in density but still outnumbered PV positive neurons in all areas. CB positive neurons found in the oldest age group, shows signs of a slow increase in both PLA and ILA while BLA shows signs of a slow decrease. The total number of CB positive neurons still exceeded that of PV positive neurons. With regard to low sample size of this project, only 6-8 animals used in each age group and 3-4 animals analyzed here, more quantitative analysis would be needed to determine if the ratio found of PV and CB positive neurons in the three areas here correlate with development and function in future findings. Bjerke et al (2021) also observed that CB positive neurons generally appear to be most numerous in areas related to emotional processing and dominant in limbic areas. Striking contrast are found between CB and PV expression at P9 where CB positive neurons starts off at high numbers and neurons expressing PV low in especially BLA. This is in line with previous findings that PV positive neurons are more abundant in motor and sensory areas (Bjerke et al., 2021) at this stage. Further, results point to large numbers of CB positive neurons found in amygdala, indicating that neurons expressing CB in this network are of high interest when studying fear memory processes. Both PV and CB patterns appear adult-like already at P14, although quantitative changes continue after that in the areas investigated here.

Alcántara and colleagues (1996) examined the neocortex of Wistar rats through different stages of development ranging from P7 to P45 and in adults. They found that the number of neurons expressing PV and CB followed different developmental patterns in rodents. Moreover, they observed colocalization of neurons expressing PV and CB peaked during the second postnatal week. The colocalization rate of neurons expressing PV and CB depended not only on the rodent's age but also on the layer of the brain examined. The authors proposed that PV and CB neurons arise from a common progenitor. In other words, neurons from the same origin expressing CB appear to shift and express PV during maturation. The data presented here indicate a similar developmental pattern and time of shift of PV and CB positive neurons in mice. Interestingly, results from this project indicates that CB neuron densities decrease while

PV positive neuron densities increase fit well with the findings by Alcantara et al (1996). The study by Alcántara et al. (1996) clarifies that quantitative analysis of anatomical features of the developing brain is necessary to fully understand how different brain regions evolve and what functions various brain regions support.

Furthermore, in the current project, we found high numbers of wide-spread CB positive neurons at early stages supporting the findings that neurons expressing CB appears and matures early (Alcántara et al., 1996). Notably, neurons expressing CB are found homogenously in BLA in early stages of development. CB positive neurons seem to decrease in density through development and appear adult-like by P21, in line with the findings of Berdel and Morys (2000) that CB positive neurons reached mature level at P21. It is not yet understood precisely why CB neuron density decreases during development, however this may be linked to various cognitive and metabolic changes that take place in the developing brain. PV positive neurons on the other hand, are found in low numbers and sparse at early stages of development correlating with findings by Alcantara et al (1994) that PV positive neurons mature noticeably late during development. Contrary to neurons expressing CB, PV was restricted in the BLA. PV positive neurons are found to build basket boutons and somatic contacts around pyramidal somata (Bähr & Wolff, 1985). These connections are efficient on the synchronization and firing activity of target neurons (Freund, 2003; Gibson et al., 1999; Klausberger T. et al., 2003; Miles et al., 1996; Tamás et al., 1997, 2000). This project's results found that PV positive neurons increase rapidly during the second postnatal week may be due to an efficient expanding network plasticity. The variances in development of neurons expressing PV and CB recognizes that they play diverse roles during maturation and development of the regions explored here (Berdel & Morys, 2000).

Worth to mention are the differences in density and total number graphs. Here, it is important to keep in mind that changes in the total number of neurons expressing PV and CB occur at the same time as the anatomical areas increase in size. While anatomical areas increase, the density of neurons will naturally decrease unless there is a simultaneous increase in the total number that outweighs the effect of the increasing area. As seen in this projects results, especially with neurons expressing CB in PLA and ILA, it seems like total number increase and density decrease. This is due to the fact that the area of the different regions are also increasing.

4.3 Fear memory and possible functional implications of development

From infancy through adolescence, changes in appearance and intelligence are noticeable daily. Neurodevelopmental changes are speculated to add increased vulnerability to a vast range of disorders that often manifest during infancy through adolescence. Disorders such as anxiety and autism are vulnerable to manifest during early stages (Ruden et al., 2021). Fear memory processes and normal function of these networks are essential through development. Among the central networks of this process are PLA, ILA and BLA and these were investigated in the current study.

PV and CB positive neurons found in this network appear to play an important role of fear expression. Inhibitory and excitatory neurons are found to work in a precise manner to control fear memory (Julien Courtin et al., 2014). PV interneurons are known to provide inhibitory inputs to control the timing of information flow and regulate synaptic excitation. Courtin et al (2014) found that activity in PV interneurons was strongly reduced during an aversive event. Consecutively, this inhibition produced strong

activation of excitatory neurons and reacting to the fear associated event driving fear behavior in the rodents. In other words, firing rate of PV interneurons were reduced during fear response suggesting that persistent fear behavior which is at the core of several neurological conditions such as anxiety disorder and PTSD may be regulated at the level of specific inhibitory circuits found in PLA, ILA and BLA. According to Muller et al (2003) such synchronization of inhibitory and excitatory networks creates a rhythmic flow during emotional arousal generated by BLA and further build the frame functions for working memory in the limbic areas and emotional memories in the amygdala. In other words, this network works closely together in fear memory processes supporting the findings of Courtin et al (2014) in PV interneurons' response to an aversive event.

Interestingly, reduced levels of neurons expressing CB in prefrontal cortex and amygdala have been shown to disrupt behavior connected to fear and anxiety. The PLA and ILA, of the prefrontal cortex, have largely distinct projection networks to the BLA (Riaz et al., 2019) which is central for fear memory processing. Harris et al (2016) suggested a compromised ability for normal interaction between PLA, ILA and BLA network connection when CB neurons are reduced. According to Riaz et al (2019), while PLA promotes the expression of fear behavior, ILA is associated with the inhibition of contextual fear behavior. PV and CB positive neurons are further believed to create a necessary frame for functions in PLA, ILA and BLA such as consolidation of emotional memories (McDonald & Mascagni, 2004) and working memory (Constantinidis et al., 2018; Lewis et al., 2005). Further, Pattwell et al (2012) suggest that a lack of synaptic plasticity in the prefrontal areas is associated with blunted regulation of fear extinction during adolescence of related to emotional processing which develop throughout adolescence of mice. By probing neural circuitry revealed altered synaptic plasticity of prefrontal areas which are modulating fear responses across development. Moreover, findings like these provide valuable insights into future treatment outcomes for timing exposure therapies and discover when treatment may be most effective during development (Pattwell et al., 2012; Szenczi et al., 2012; Wilkinson et al., 2016; Fairless et al., 2019).

Thus, research continue to find decreased levels of these neurons in several neurological conditions such as anxiety, autism and more (Courtin et al., 2014; Harris et al., 2016; Page et al., 2019), indicating that PV and CB positive neurons may have a role in fear extinction and anxiety disorders (Šutulović et al., 2021). Altogether, dysfunction of the fear memory network caused by altered expression of CB and PV may lead to disruption of normal fear memory sprocesses. However, so far our knowledge about the density and number of neurons expressing PV and CB across the developing brain has been limited to few regions and fragmented, due to methodological approach and criteria used to define regions of interest significantly affect results (Bjerke et al., 2020). The findings of this thesis indicate that the balance between PV and CB cell numbers in this network change drastically during development, and a precise tuning of this balance may be instrumental for normal development. Findings further support the importance of PV and CB positive neurons in normal function and refer to dysfunction when the expression of CBP is reduced in these areas. Future work may also examine the possibility to regulate activity at the level of specific inhibitory circuits when treating neurodevelopmental diseases such as anxiety disorders. In addition, a large collection of brain wide data from this project has been shared through EBRAINS, and this thesis gives a proof of concept that the data can yield biologically useful findings. Shared data are available for future research on maturation of brain regions not only limited to fear memory circuitry.

4.4 Relevance of the mouse model to human development

Murine models are widely popular in research on human health and body. Almost 99% of genes resemble the human genome (Dutta & Sengupta, 2016). Laboratory mice have a pregnancy period of about 20 days and a lifespan of about 24 months (Dutta & Sengupta, 2016). The murine model is therefore highly convenient for research when exploring developmental processes. However, Dutta and Sengupta (2016) concluded that the gap between approximation and accuracy differed significantly and the set age correlation does not apply without considering each phase of life separately. In other words, this age correlation varies depending on the precise correlation between mice and human age at a specific phase of life. In this project, the age group ranges from postnatal day 9 up to postnatal day 35 which could represent a comparable line from infancy up to early puberty stage in humans when considering developmental factors. A murine brain is less mature at birth, corresponding to a human prenatal brain when comparing cross-species differences. Nine days in mice is equivalent to one human year while 2 years equals to 80 years of a human.

4.5 Future directions

This study investigated the development of PV and CB positive neurons in areas related to fear memory processes. The project has generated a collection of data including more than 2500 images mapping the development pattern of neurons expressing PV and CB. However, the final data used for quantitative analysis is limited, originating from a total of 30 animals in four different age groups. Thus, conclusions at this point are tentative and future studies with more animals should build on this data to verify the results found here. The extensive data resulting from this project will be openly shared through the EBRAINS Knowledge Graph to facilitate such re-analysis and re-use.

Resulting data will allow for discussion regarding CB and PV evolving model and examine areas that might reach adult like structures before others. An interesting factor that was not considered in this project is the neuroanatomical developmental sex differences. Qiu et al (2018) discovered that regions larger in males advance earlier than those larger in females. Further, Harris et al (2016) found that females had higher expression than males in amygdala and the opposite was true for the PFC where PLA and ILA are located. This suggest that sex differences in amount of CB positive neurons found in these areas through development influence behavior (Harris et al., 2016). In line with this, research has also indicated that PV positive neurons in PFC areas, such as PLA and ILA, in male mice are more resilient to manipulations than in females, suggesting functional dimorphism (Page et al., 2019). To elaborate, these latter authors further reported that male mice also need a longer duration of stress exposure to activate an anxiety-like behavior. Suggesting that sex-specific circuits may play a role in the mediation of anxiety related behaviors and disorders connected to PV and CB positive neurons. Insights on this topic opens up possibilities to offer answers to biologically relevant questions beyond the ones covered here such as examining functional properties, network construction, and neurodevelopmental diseases.

5 Conclusion

This project investigated the development pattern of parvalbumin (PV) and calbindin (CB) positive neurons in three anatomical areas related to fear memory in mice aging from P9 through P35. Results indicated interesting data for the development pattern of neurons expressing PV and CB found in the four age groups analyzed. The

main finding was an increase in PV positive neurons from early age while CB positive neurons decreased. Furthermore, both appear adult-like between P14 and P21. Brain wide data resulting from this project will be shared through EBRAINS and can be used for other research.

References

Abercrombie, M. (1946). The Annotated Abercrombie. *The Anatomical Record*, *94*, 239–247.

Ahn, J., Hong, S., Park, J., Kim, I., Cho, J., Lee, T., Lee, J., Chen, B., Shin, B., Bae, E., Jeon, Y., Kim, Y., Won, M., & Choi, S. (2017). Immunoreactivities of calbindin-D28k, calretinin and parvalbumin in the somatosensory cortex of rodents during normal aging. *Molecular Medicine Reports*, *16*(5), 7191–7198. https://doi.org/10.3892/mmr.2017.7573

Alcántara, S., De Lecea, L., Del Río, J., Ferrer, I., & Soriano, E. (1996). Transient colocalization of parvalbumin and calbindin D28k in the postnatal cerebral cortex: Evidence for a phenotypic shift in developing nonpyramidal neurons. *European Journal of Neuroscience*, *8*(7), 1329–1339. https://doi.org/10.1111/j.1460-9568.1996.tb01595.x

Alcántara, S., & Ferrer, I. (1994). Postnatal development of parvalbumin immunoreactivity in the cerebral cortex of the cat. *The Journal of Comparative Neurology*, *348*(1), 133–149. https://doi.org/10.1002/cne.903480108

Bähr, S., & Wolff, J. R. (1985). Postnatal development of axosomatic synapses in the rat visual cortex: Morphogenesis and quantitative evaluation. *The Journal of Comparative Neurology*, *233*(3), 405–420.

Berdel, B., & Morys, J. (2000). Expression of calbindin-D28k and parvalbumin during development of rat's basolateral amygdaloid complex. *International Journal of Developmental Neuroscience*, *18*(6), 501–513.

Berridge, M. (1998). Neuronal calcium. *Neuronal Calcium Signaling*, *21*(13–26), 26. https://doi.org/10.1016/0166-2236(87)90099-3

Bjerke, I., Yates, S., Laja, A., Witter, M., Puchades, M., Bjaalie, J., & Leergaard, T. (2021). Densities and numbers of calbindin and parvalbumin positive neurons across the rat and mouse brain. *IScience*, *24*(1), 101906. https://doi.org/10.1016/j.isci.2020.101906

Bjerke, I., Yates, S., Puchades, M., Bjaalie, J., & Leergaard, T. (2020). *Brain-wide quantitative data on parvalbumin positive neurons in the mouse*. EBRAINS. https://doi.org/10.25493/BT8X-FN9

Brust, V., Schindler, P. M., & Lewejohann, L. (2015). Lifetime development of behavioural phenotype in the house mouse (Mus musculus). *Frontiers in Zoology*, *12*(1), 1–14. https://doi.org/10.1186/1742-9994-12-S1-S17

Constantinidis, C., Funahashi, S., Lee, D., Murray, J. D., Qi, X. L., Wang, M., & Arnsten, A. F. T. (2018). Persistent spiking activity underlies working memory. *Journal of Neuroscience*, *38*(32), 7020–7028. https://doi.org/10.1523/JNEUROSCI.2486-17.2018

Courtin, Julien, Chaudun, F., Rozeske, R. R., Karalis, N., Gonzalez-Campo, C., Wurtz, H., Abdi, A., Baufreton, J., Bienvenu, T. C. M., & Herry, C. (2014). Prefrontal parvalbumin interneurons shape neuronal activity to drive fear expression. *Nature*, *505*(7481), 92–96. https://doi.org/10.1038/nature12755

Desgent, S., Boire, D., & Ptito, M. (2010). Altered expression of parvalbumin and calbindin in interneurons within the primary visual cortex of neonatal enucleated

hamsters. *Neuroscience*, *171*(4), 1326–1340. https://doi.org/10.1016/j.neuroscience.2010.10.016

Dimmock & Lawlor. (2017). Cellular and molecular introduction ot brain deve. *Neurobiology of Disease*, *176*(12), 139–148. https://doi.org/10.1016/j.nbd.2015.07.007.Cellular

Dutta, S., & Sengupta, P. (2016). Men and mice: Relating their ages. In *Life Sciences* (Vol. 152, pp. 244–248). Elsevier Inc. https://doi.org/10.1016/j.lfs.2015.10.025

Elíes, J., Yáñez, M., Pereira, T. M. C., Gil-Longo, J., MacDougall, D. A., & Campos-Toimil, M. (2020). An Update to Calcium Binding Proteins. In *Advances in Experimental Medicine and Biology* (Vol. 1131). https://doi.org/10.1007/978-3-030-12457-1_8

Evans, R. C., & Blackwell, K. T. (n.d.). *Calcium: Amplitude, Duration, or Location?*

Fairless, R., Williams, S. K., & Diem, R. (2019). Calcium-binding proteins as determinants of central nervous system neuronal vulnerability to disease. *International Journal of Molecular Sciences*, *20*(9), 1–14. https://doi.org/10.3390/ijms20092146

Ferguson, B. R., & Gao, W. J. (2018). Pv interneurons: critical regulators of E/I balance for prefrontal cortex-dependent behavior and psychiatric disorders. *Frontiers in Neural Circuits*, *12*(May), 1–13. https://doi.org/10.3389/fncir.2018.00037

Freund, T. F. (2003). Interneuron Diversity series: Rhythm and mood in perisomatic inhibition. *Trends in Neurosciences*, *26*(9), 489–495. https://doi.org/10.1016/S0166-2236(03)00227-3

Gattoni, G., & Bernocchi, G. (2019). Calcium-Binding Proteins in the Nervous System during Hibernation: Neuroprotective Strategies in Hypometabolic Conditions? *International Journal of Molecular Sciences*, *20*(9), 2364. https://doi.org/10.3390/ijms20092364

Gibson, J. R., Beierlein, M., & Connors, B. W. (1999). *47035*. *402*(November), 75–79.

Gonzalez-Burgos, G., Cho, R. Y., & Lewis, D. A. (2015). Alterations in cortical network oscillations and parvalbumin neurons in schizophrenia. *Biological Psychiatry*, *77*(12), 1031–1040. https://doi.org/10.1016/j.biopsych.2015.03.010

Harris, E. E. P., Abel, J. J. M., Tejada, L. L. D., & Rissman, E. E. F. (2016). Calbindin knockout alters sex-specific regulation of behavior and gene expression in amygdala and prefrontal cortex. *Endocrinology*, *157*(5), 1967–1979. https://doi.org/10.1210/en.2016-1055

Hof, P. R., Glezer, I. I., Condé, F., Flagg, R. A., Rubin, M. B., Nimchinsky, E. A., & Vogt Weisenhorn, D. M. (1999). Cellular distribution of the calcium-binding proteins parvalbumin, calbindin, and calretinin in the neocortex of mammals: Phylogenetic and developmental patterns. In *Journal of Chemical Neuroanatomy* (Vol. 16, Issue 2, pp. 77–116). Elsevier. https://doi.org/10.1016/S0891-0618(98)00065-9

Hu, H., Gan, J., & Jonas, P. (2014). Fast-spiking, parvalbumin^{+} GABAergic interneurons: From cellular design to microcircuit function. *Science*, *345*(6196). https://doi.org/10.1126/science.1255263

Izquierdo, I., Furini, C. R. G., & Myskiw, J. C. (2016). Fear memory. *Physiological Reviews*, *96*(2), 695–750. https://doi.org/10.1152/physrev.00018.2015

Jinno, S., & Kosaka, T. (2006). Cellular architecture of the mouse hippocampus: a quantitative aspect of chemically defined GABAergic neurons with stereology. *Neurosci Res*, *56*(3), 229–245.

Jones, R. S. G., & Bühl, E. H. (1993). Basket-like interneurones in layer II of the entorhinal cortex exhibit a powerful NMDA-mediated synaptic excitation. *Neuroscience Letters*, *149*(1), 35–39.

Kawaguchi, Y., Katsumaru, H., Kosaka, T., Heizmann, C. W., & Hama, K. (1987). Fast spiking cells in rat hippocampus (CA1 region) contain the calcium-binding protein parvalbumin. *Brain Research*, *416*(2), 369–374.

Kemppainen, S., & Pitkänen, A. (2000). Distribution of parvalbumin, calretinin, and calbindin-D28k immunoreactivity in the rat amygdaloid complex and colocalization with γ-aminobutyric acid. *Journal of Comparative Neurology*, *426*(3), 441–467.

Klausberger T., Magill PJ, Marton LF, Roberts JDB, Cobden PM, Buzsaki G, & P., S. (2003). Brain-state- and cell-type-specific firing of hippocampal interneurons in vivo. *Nature*, *421*(6925), 844–848.

Legaz, I., Olmos, L., Real, M. Á., Guirado, S., Dávila, J. C., & Medina, L. (2005). Development of neurons and fibers containing calcium binding proteins in the pallial amygdala of mouse, with special emphasis on those of the basolateral amygdalar complex. *Journal of Comparative Neurology*, *488*(4), 492–513. https://doi.org/10.1002/cne.20608

Lewis, S. G., Slabosz, A., Robbins, T. W., Barker, R. A., & Owen, A. M. (2005). Dopaminergic basis for deficits in working memory but not attentional set-shifting in Parkinson's disease. *Neuropsychologia*, *43*(6), 823–832. https://doi.org/10.1016/j.neuropsychologia.2004.10.001

Lübke, J., Geiger, J. R. P., Ceranik, K., Bender, R., Monyer, H., Frotscher, M., & Jonas, P. (1997). A novel type of GABAergic interneuron connecting the input and the output regions of the hippocampus. *Journal of Neuroscience*, *17*(14), 5380–5394. https://doi.org/10.1523/jneurosci.17-14-05380.1997

Markram, H., Toledo-Rodriguez, M., Wang, Y., Gupta, A., Silberberg, G., & Wu, C. (2004). Interneurons of the neocortical inhibitory system. *Nature Reviews Neuroscience*, *5*(10), 793–807. https://doi.org/10.1038/nrn1519

McCormick, D. A., Connors, B. W., Lighthall, J. W., & Prince, D. A. (1985). Comparative electrophysiology of pyramidal and sparsely spiny stellate neurons of the neocortex. *Journal of Neurophysiology*, *54*(4), 782–806. https://doi.org/10.1152/jn.1985.54.4.782

McDonald, A. J., & Mascagni, F. (2004). Parvalbumin-Containing Interneurons in the Basolateral Amygdala Express High Levels of the α1 Subunit of the GABAA Receptor. *Journal of Comparative Neurology*, *473*(1), 137–146. https://doi.org/10.1002/cne.20101

McMahon, A., Wong, B. S., Iacopino, A. M., Ng, M. C., Chi, S., & German, D. C. (1998). Calbindin-D(28k) buffers intracellular calcium and promotes resistance to degeneration in PC12 cells. *Molecular Brain Research*, *54*(1), 56–63. https://doi.org/10.1016/S0169-328X(97)00305-7

Medina, L., Abellán, A., Vicario, A., & Desfilis, E. (2014). Evolutionary and Developmental Contributions for Understanding the Organization of the Basal Ganglia. *Brain,*

Behavior and Evolution, *83*(2), 112–125. https://doi.org/10.1159/000357832

Miao, C, Cao, Q., Moser, M., & Moser, E. (2017). Parvalbumin and Somatostatin Interneurons Control Different Space-Coding Networks in the Medial Entorhinal Cortex. *Cell*, *171*(3), 507–521. https://doi.org/10.1016/j.cell.2017.08.050

Miao, Chao, Humphrey, R. H., & Qian, S. (2017). A meta-analysis of emotional intelligence effects on job satisfaction mediated by job resources, and a test of moderators. *Personality and Individual Differences*, *116*, 281–288. https://doi.org/10.1016/j.paid.2017.04.031

Miles, R., Tóth, K., Gulyás, A., Hájos, N., & Freund, T. (1996). Differences between Somatic and Dendritic Inhibition in the Hippocampus. *Neuron*, *16*, 815–823.

Molinari, S., Battini, R., Ferrari, S., Pozzi, L., Killcross, A. S., Robbins, T. W., Jouvenceau, A., Billard, J. M., Dutar, P., Lamour, Y., Baker, W. A., Cox, H., & Emson, P. C. (1996). Deficits in memory and hippocampal long-term potentiation in mice with reduced calbindin D28K expression. *Proceedings of the National Academy of Sciences of the United States of America*, *93*(15), 8028–8033. https://doi.org/10.1073/pnas.93.15.8028

Mukherjee, A., & Caroni, P. (2018). Infralimbic cortex is required for learning alternatives to prelimbic promoted associations through reciprocal connectivity. *Nature Communications*, *9*(1). https://doi.org/10.1038/s41467-018-05318-x

Muller, J. F., Mascagni, F., & McDonald, A. J. (2003). Synaptic connections of distinct interneuronal subpopulations in the rat basolateral amygdalar nucleus. *Journal of Comparative Neurology*, *456*(3), 217–236. https://doi.org/10.1002/cne.10435

Nelson, M. R., & Chazin, W. J. (1998). An interaction-based analysis of calcium-induced conformational changes in Ca2+ sensor proteins. *Protein Science*, *7*(2), 270–282. https://doi.org/10.1002/pro.5560070206

Newmaster, K. T., Nolan, Z. T., Chon, U., Vanselow, D. J., Weit, A. R., Tabbaa, M., Hidema, S., Nishimori, K., Hammock, E. A. D., & Kim, Y. (2020). Quantitative cellular-resolution map of the oxytocin receptor in postnatally developing mouse brains. *Nature Communications*, *11*(1), 1–12. https://doi.org/10.1038/s41467-020-15659-1

Nieves, G. M., Bravo, M., Baskoylu, S., & Bath, K. G. (2020). Early life adversity decreases pre-adolescent fear expression by accelerating amygdala PV cell development. *ELife*, *9*, 1–24. https://doi.org/10.7554/eLife.55263

Packer, A. M., & Yuste, R. (2011). Dense, unspecific connectivity of neocortical parvalbumin-positive interneurons: A canonical microcircuit for inhibition? *Journal of Neuroscience*, *31*(37), 13260–13271. https://doi.org/10.1523/JNEUROSCI.3131-11.2011

Page, C. E., Shepard, R., Heslin, K., & Coutellier, L. (2019). prefrontal parvalbumin cells are sensitive to stress and mediate anxiety-related behaviors in female mice. *Scientific Reports*, *9*(19772). https://doi.org/10.1038/s41598-019-56424-9

Pattwell, S. S., Duhoux, S., Hartley, C. A., Johnson, D. C., Jing, D., Elliott, M. D., Ruberry, E. J., Powers, A., Mehta, N., Yang, R. R., Soliman, F., Glatt, C. E., Casey, B. J., Ninan, I., & Lee, F. S. (2012). Altered fear learning across development in both mouse and human. *Proceedings of the National Academy of Sciences of the United States of America*, *109*(40), 16318–16323.

https://doi.org/10.1073/pnas.1206834109

Qiu, L. R., Fernandes, D. J., Szulc-Lerch, K. U., Dazai, J., Nieman, B. J., Turnbull, D. H., Foster, J. A., Palmert, M. R., & Lerch, J. P. (2018). Mouse MRI shows brain areas relatively larger in males emerge before those larger in females. *Nature Communications*, *9*(1). https://doi.org/10.1038/s41467-018-04921-2

Reynolds, G. P., Abdul-Monim, Z., Neill, J. C., & Zhang, Z. J. (2004). Calcium binding protein markers of GABA deficits in schizophrenia - Post mortem studies and animal models. *Neurotoxicity Research*, *6*(1), 57–61. https://doi.org/10.1007/BF03033297

Riaz, S., Puveendrakumaran, P., Khan, D., Yoon, S., Hamel, L., & Ito, R. (2019). Prelimbic and infralimbic cortical inactivations attenuate contextually driven discriminative responding for reward. *Scientific Reports*, *9*(1), 1–13. https://doi.org/10.1038/s41598-019-40532-7

Ruden, J. B., Dugan, L. L., & Konradi, C. (2021). Parvalbumin interneuron vulnerability and brain disorders. *Neuropsychopharmacology*, *46*(2), 279–287. https://doi.org/10.1038/s41386-020-0778-9

Rudy, B., Fishell, G., Lee, S., & Hjerling-Leffler, J. (2011). Three groups of interneurons account for nearly 100% of neocortical GABAergic neurons. *Developmental Neurobiology*, *71*(1), 45–61. https://doi.org/10.1002/dneu.20853

Sakai, T., Oshima, A., Nozaki, Y., Ida, I., Haga, C., Akiyama, H., Nakazato, Y., & Mikuni, M. (2008). Changes in density of calcium-binding-protein-immunoreactive GABAergic neurons in prefrontal cortex in schizophrenia and bipolar disorder. *Neuropathology*, *28*(2), 143–150. https://doi.org/10.1111/j.1440-1789.2007.00867.x

Schmidt-Kastner, R., Meller, D., & Eysel, U. T. (1992). Immunohistochemical changes of neuronal calcium-binding proteins parvalbumin and calbindin-D-28k following unilateral deafferentation in the rat visual system. *Experimental Neurology*, *117*(3), 230–246. https://doi.org/10.1016/0014-4886(92)90132-A

Schulreich, S., Gerhardt, H., Meshi, D., & Heekeren, H. R. (2020). Fear-induced increases in loss aversion are linked to increased neural negative-value coding. *Social Cognitive and Affective Neuroscience*, *15*(6), 661–670. https://doi.org/10.1093/scan/nsaa091

Schwaller, B. (2020). Cytosolic Ca2+ buffers are inherently Ca2+ signal modulators. *Cold Spring Harbor Perspectives in Biology*, *12*(1). https://doi.org/10.1101/cshperspect.a035543

Sharpe, M. J., & Killcross, S. (2015). The prelimbic cortex uses higher-order cues to modulate both the acquisition and expression of conditioned fear. *Frontiers in Systems Neuroscience*, *8*(JAN), 1–10. https://doi.org/10.3389/fnsys.2014.00235

Sohal, V. S., Zhang, F., Yizhar, O., & Deisseroth, K. (2009). Parvalbumin neurons and gamma rhythms enhance cortical circuit performance. *Nature*, *459*(7247), 698–702. https://doi.org/10.1038/nature07991

Šutulović, N., Grubač, Ž., Šuvakov, S., Jerotić, D., Puškaš, N., MacUt, D., Rašić-Marković, A., Simić, T., Stanojlović, O., & Hrnčić, D. (2021). Experimental Chronic Prostatitis/Chronic Pelvic Pain Syndrome Increases Anxiety-Like Behavior: The Role of Brain Oxidative Stress, Serum Corticosterone, and Hippocampal Parvalbumin-Positive Interneurons. *Oxidative Medicine and Cellular Longevity*, *2021*.

https://doi.org/10.1155/2021/6687493

Szabadics, J., Varga, C., Brunner, J., Chen, K., & Soltesz, I. (2010). Granule cells in the CA3 area. *Journal of Neuroscience*, *30*(24), 8296–8307. https://doi.org/10.1523/JNEUROSCI.5602-09.2010

Szenczi, P., Bánszegi, O., Groó, Z., & Altbäcker, V. (2012). Development of the Social Behavior of Two Mice Species With Contrasting Social Systems. *Aggressive Behavior*, *38*(4), 288–297. https://doi.org/10.1002/ab.21431

Takahashi, T., Nowakowski, R. S., & Caviness, V. S. (1996). The leaving or Q fraction of the murine cerebral proliferative epithelium: A general model of neocortical neuronogenesis. *Journal of Neuroscience*, *16*(19), 6183–6196. https://doi.org/10.1523/jneurosci.16-19-06183.1996

Tamás, G., Buhl, E. H., & Somogyi, P. (1997). Fast IPSPs elicited via multiple synaptic release sites by different types of GABAergic neurone in the cat visual cortex. *Journal of Physiology*, *500*(3), 715–738. https://doi.org/10.1113/jphysiol.1997.sp022054

Tamás, G., Buhl, E., Lőrincz, A., & Somogyi, P. (2000). Proximally targeted GABAergic synapses and gap juctions synchronize cortical interneurons. *Nature Neuroscience*, *3*(4), 1–6.

Trutzer, I. M., García-Cabezas, M. Á., & Zikopoulos, B. (2019). Postnatal development and maturation of layer 1 in the lateral prefrontal cortex and its disruption in autism. *Acta Neuropathologica Communications*, *7*(1), 40. https://doi.org/10.1186/s40478-019-0684-8

Tyzio, R., Represa, A., Jorquera, I., Ben-Ari, Y., Gozlan, H., & Aniksztejn, L. (1999). The establishment of GABAergic and glutamatergic synapses on CA1 pyramidal neurons is sequential and correlates with the development of the apical dendrite. *The Journal of Neuroscience*, *19*(23), 10372–10382.

Wilkinson, M., Dumontier, M., Aalbersberg, I., Appleton, G., Axton, M., Baak, A., Blomberg, N., Boiten, J.-W., da Silva Santos, L., Bourne, P., Bouwman, J., Brookes, A., Clark, T., Crosas, M., Dillo, I., Dumon, O., Edmunds, S., Evelo, C., Finkers, R., … Mons, B. (2016). The FAIR Guiding Principles for scientific data management and stewardship. *Scientific Data*, *3*, 1–9. https://doi.org/10.1038/sdata.2016.18

Wouterlood, F. G., Härtig, W., Brückner, G., & Witter, M. P. (1995). Parvalbumin-immunoreactive neurons in the entorhinal cortex of the rat: localization, morphology, connectivity and ultrastructure. *Journal of Neurocytology*, *24*(2), 135–153. https://doi.org/10.1007/BF01181556

Young, M. B., & Thomas, S. A. (2014). M1-muscarinic receptors promote fear memory consolidation via phospholipase C and the M-current. *Journal of Neuroscience*, *34*(5), 1570–1578. https://doi.org/10.1523/JNEUROSCI.1040-13.2014

Zheng, S., Chan, W. S., Leung, S. H., & Xue, Q. (2007). Broadband Butler matrix with flat coupling. *Electronics Letters*, *43*(10), 576–577. https://doi.org/10.1049/el:20070274

Appendix

Appendix A: Perfusion protocol

Appendix B: Immunohistochemistry protocol

Appendix C: Perfusion parameters

Appendix A: Perfusion protocol

INTRACARDIAL PERFUSION OF RODENTS FOR LIGHT MICROSCOPY ANALYSIS

Stepwise description of perfusion technique
Preparation of 4% Paraformaldehyde in 0,1 M NaPi pH 7,4
Preparation of 2-4% Dextran in 0,1 M NaPi pH 7,4

Protocol prepared by Eystein Hellstrøm Hoddevik 22.06.09, revised 04.08.11

1. <u>The day prior to performing the procedure: booking and preparation of fixative:</u>
First, book the necessary intervention room, and book a perfusion pump.

Prepare the fixative solution the day prior. Preparation time: approx 1-1,5 hours.

2. <u>Choosing a fixative:</u>
For electron microscopy analysis, use one of the following (see separate protocols):

- pH shift protocol (can also be used for light microscopy)
- 4% PFA + 0,1% GA (glutaraldehyde)
- 4% PFA + 0,5% GA
- 1% PFA + 2,5% GA

For specimens that will only be used for light microscopy, prepare 4% Paraformaldehyde in 0,1 M NaPi, pH 7,4 as follows:

<u>*Solution A*</u>:
should be prepared under a vent

Dissolve 11,5 g Na_2HPO_4 (Mw 141,96) in approx 600 mL of ddH_2O

Add 40 g of paraformaldehyde

Add magic stirrer, place the solution on a heating plate, the temperature can be set to between 100 and 150, this will result in a satisfactory temperature for the solution (not exceeding 70 ^{0}C). Takes approx 1 hour to dissolve.

<u>*Solution B:*</u>
Add 2,3 g NaH_2PO_4 to approx 200 mL ddH_2O

Mix both solutions and adjust final volume, with ddH_2O, to 1000 mL

Filter the resultant solution (to eliminate precipitates that would otherwise become micro-emboli and reduce the quality of perfusion).

The final solution should have a pH of 7,4 (physiological pH) and pH adjustment should not be required (unless you've added significant amounts of NaOH to solution A in order for the PFA to dissolve quicker).

Using a 50mL Falcon tube, prepare 2% or 4% solution of Dextran, mixed in NaPi. For example:

<u>*Dextran solution 2% in 0,1M NaPi pH 7,4*</u>
Add 0,8 g dextran to approx 30 mL of NaPi, adjust final volume to 40 mL.

3. Make sure all the necessary equipment is available:.
an infusion pump and wire (remember to book this the day prior)

blunt cannulae for intracardial
injections sharp cannulae for
anaesthesia syringes of 1 mL
volume,

anaesthesia (usually phenobarbitol) - equthesin

containers for brains, a
pen for marking, a timer
(to calibrate the pump),

a dissection scissor and foreceps (blunt and with
teeth) gloves

a small container of ethanol

4. Practical set-up in the laboratory area:
Board and needles: A board must be available, with needles in sufficient number to fix the animal. Make sure this board is placed in such a way that it can easily be held in place without moving when the dissection commences. Used PFA solution must be collected and dealt with accordingly. Use a plastic tray to collect the used fixative.

Pump and fixative: Install the container (bottle) with freshly prepared fixative solution. For mice, ensure the pumps delivers 6-8 mL per min, which should be titrated with H_20 prior to commencing, unless already done. The infusion tube needs to be completely void of bubbles, so as to avoid inadequate perfusion and air emboli.

Cold dextran IV: For any infusion of an animal, the first volume injected should contain ice cold dextran – with the purpose of dilating blood vessels and assuring a more profuse infusion. Infuse with dextran for approx 20 seconds. Keep the Dextran solution in a Falcon tube, and reverse the pump direction on the peristalsis pump to draw up ice cold Dextran just prior to perfusion.

There is some debate as to which temperature the fixative solution should hold. Ensure that it does not exceed room temperature. Alternatively, use cold fixative, approx 4 ^{0}C.

5. Performing the anaesthesia
The most commonly used anesthesia involves an intraperitoneal injection of pentobarbital. For an adult mouse, approx 130-150 uL of Equthesin is needed.

Assess whether the mouse is anesthetised: assess response to pain in extremities, tail, or examine the corneal reflex (should be absent). When adequately anaesthetised, proceed to fixing the animal to the polyethylene board prior to dissection.

6. Performing the dissection and perfusion
a.Midline peritoneal dissection, then thoracic dissection. Apply some ethanol on to the belly. With the animal anaesthetised, lying on its back, the first incision should be made with the dissection scissors into the peritoneal cavity. Continue with a midline incision, exposing first the xiphisternum, then continue laterally in two separate incision through the thoracic cavity, thus exposing the heart and lungs.

b. Swift action once thoracic cavity is exposed: From the point where the thorax is dissected, one should move swiftly, simply because general hypoxia will ensue shortly thereafter, with subsequent cardiac arrest.

c: Adequate exposure of intrathoracic structures: Ensure that all intrathoracic structures, particularly the heart, are adequately exposed. The older the animal gets, the greater the pericardial deposition of fat. This is negligeable in younger animals.

d.Incision into R atrium: In order to ex-sanguinate the heart, a small incision into the R atrium must be made.

e. Insertion of blunt cannula into L ventricle: The cannula is blunt for the reason that a sharp structure would penetrate any structure in the heart. It needs to be placed in the L ventricle. Start the pump before inserting the cannula, hold the heart with a blunt pair of foreceps and insert the cannula. Once inserted, the tip of the cannula should be placed in the aorta for optimal perfusion of the CNS, and you should visualise the tip in the aorta. Do not use force when advancing the cannula, if there is 'backflow' of fixative from the insertion site, the cannula might be placed against the heart wall – in which case you may withdraw the needle slightly

The signs of having succeeded in a technically satisfactory perfusion are:

- A pale liver
- Prompt neck stiffness and myoclonus (cramps).
- Upon cutting of the nose of the animal, a drop of fixative will gradually appear - A similar drop will appear upon cutting the tail.

7. Dissection to remove brain and central nervous system

Once the perfusion has been performed satisfactorily, the animal can be decapitated at the level of the shoulders. Try to conserve the rostral part of the spinal cord.

Initially dissect through the skin in the midline. Identify the occiput, and make two oblique incisions lateral to the occiput. When lifting the skull bone, use the flat side of the scissors towards the CNS, and lift upwards in a tangential fashion so that the brain will not get damaged. The most robust part of the rodent skull is that over the frontal/olfactory lobes.

When the CNS is adequately exposed, turn the head upside down and cut the cranial nerves, seen as white fibres protruding from the CNS, including the optic nerves. This should free the CNS from the cranium.

8. Conservations in paraformaldehyde solutions

The organs/tissue material removed should be post-fixed in perfusion fixative overnight, then stored in a dilution of 1:10 PFA (dilute in NaPi, to maintain the physiological salt concentrations). This can be kept for a significant period of time, in 4 ^{0}C

Appendix B: Immunohistochemistry protocol

All steps was performed at room temperature unless otherwise specified.

Day 1

1.	Wash with **PBS**	3x10 min
2.	Blocking with **PBS w/ 3% H2O2** (make fresh same day)	5 min
3.	Wash with **PBS**	3x5 min
4.	Blocking in **PBS w/ 10% NDS, 1% BSA, .5% trx**	1 h
5.	Primary antibody incubation in **PBS w/ 3% NDS, 1% BSA, .1% trx** box	o/n in fridge

Day 2

6.	Wash with **PBS w/ .2% trx**	3x10 min
7.	Secondary antibody incubation in **PBS w/ 3% NDS, 1% BSA, .1% trx**	1 h
8.	Wash with **PBS w/ .2% trx**	2x10 min
9.	Wash with **PBS**	10 min
10.	Wash with **ABC** (prepare 30 min before use in **PBS**)	30 min
11.	Wash with **PBS w/ .2% trx**	2x10 min
12.	Wash with **PBS**	10 min
13.	Chromogenic reaction with **DAB-kit** (prepare right before use)	
14.	Stop reaction with sterile **MQ water**	2x5 min
15.	Wash with **PBS**	10 min
16.	Mounting from NAPI or fresh PBS onto gelatinized slides	
17.	Air dry	
18.	Dehydrate with **70%, 96%, 100% etanol, xylene**	2 min each
19.	Coverslipping with **Eukitt** same day	

Appendix C: Perfusion parameters

ID	Sex	Age group	Age (in days)	Weight (g)	Perfusion status	Used in current analysis
865	M	35	34	18,30	Medium	
192	M	35	34	18,23	Good	Yes
486	M	35	34	20,05	Good	
532	M	35	34	17,86	Good	Yes
514	M	35	34	19,80	Good	
617	M	35	34	17,35	Medium	
860	M	35	35	18,59	Bad	
708	M	35	35	18,20	Good	Yes
172	M	35	35	20,00	Good	Yes
600	M	35	35	19,60	Bad	
900	M	35	35	18,35	Bad	
658	M	35	35	17,89	Medium	
717	M	9	9	5,41	Good	
274	M	9	9	5,97	Medium	Yes
857	F	9	9	5,72	Good	
431	F	9	9	6,06	Good	Yes
693	F	9	9	6,10	Good	Yes
612	F	9	9	5,50	Good	
518	M	9	9	5,00	Bad	Yes
576	M	9	9	5,50	Good	
864	M	14	14	5,70	Pink	
878	M	14	14	5,65	Good	Yes
205	M	14	14	4,70	Pink	Yes
104	M	14	14	5,90	Good	Yes
562	F	14	14	5,80	Good	
720	F	14	14	5,30	Good	
127	M	21	21	7,80	Good	Yes
558	M	21	21	7,70	Bad	
134	M	21	21	7,00	Good	
735	F	21	21	8,00	Good	
311	F	21	21	7,50	Good	
178	F	21	21	8,00	Good	Yes
466	M	21	22	8,00	Good	
137	M	21	22	7,40	Good	Yes
255	F	21	22	7,00	Good	
883	F	21	22	7,30	Good	
817	F	21	22	7,40	Good	
704	F	21	22	7,40	Good	
488	F	14	14	8,00	Good	
550	F	14	14	7,30	Good	
279	F	14	14	5,00	Bad	
276	M	14	14	9,00	Good	
214	M	14	14	5,80	Good	

399	M	9	9	4,50	Good	
370	F	9	9	4,20	Good	
239	M	17	17	6,60	Good	
124	M	17	17	6,50	Good	
390	M	17	17	5,60	Bad	
988	M	17	17	7,00	Good	
774	F	17	17	5,70	Good	
295	F	17	17	6,70	Good	
251	F	17	17	7,20	Good	
746	M	28	28	15,70	Good	
383	M	28	28	14,90	Good	
257	M	28	28	14,60	Good	
367	M	28	28	13,50	Good	
607	M	28	28	14,80	Good	
809	M	28	28	14,00	Good	
815	F	35	35	19,60	Good	
110	F	35	35	18,10	Good	
650	F	35	35	17,80	Bad	
449	F	35	35	17,10	Bad	
111	F	35	35	18,40	Good	

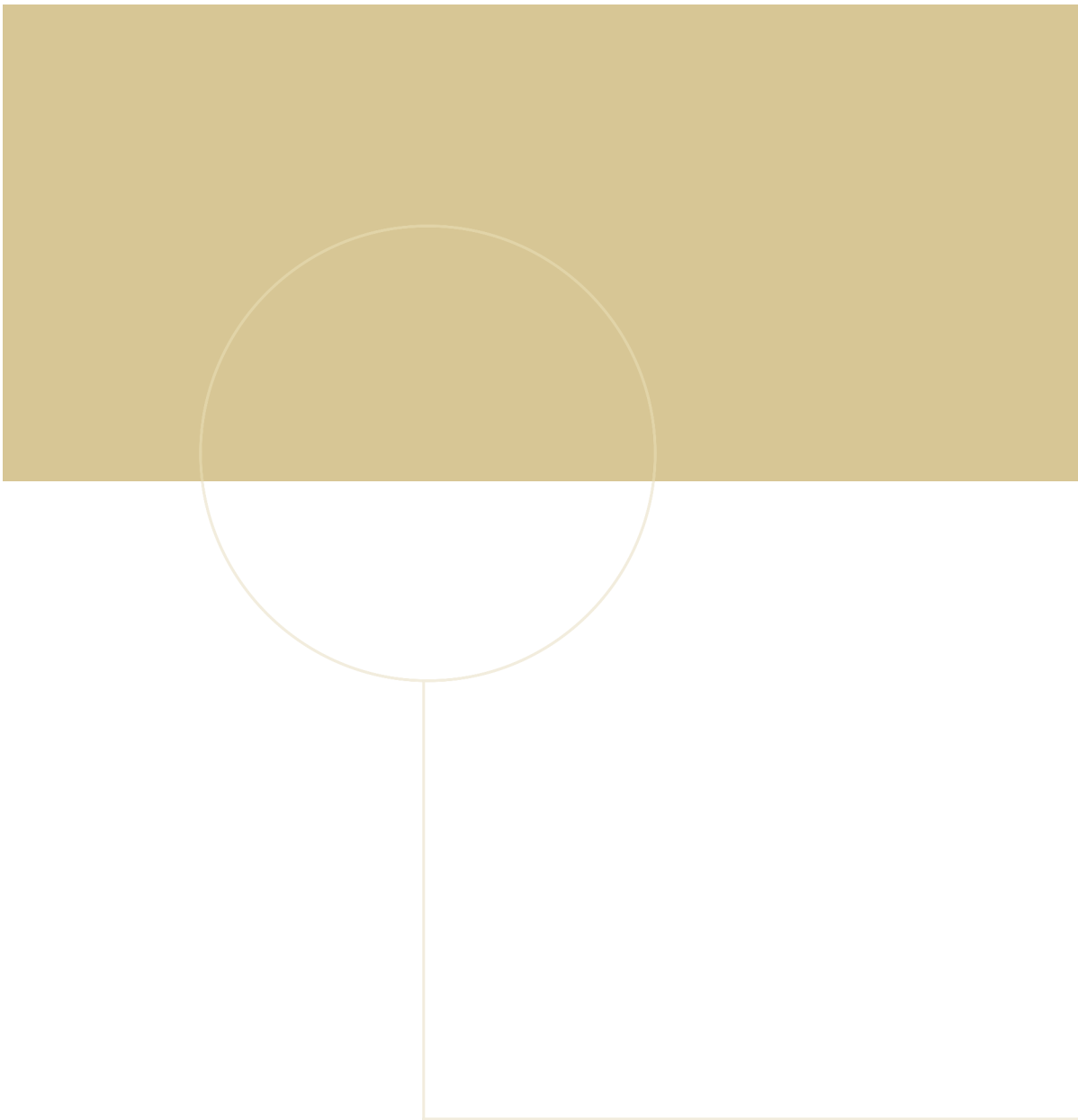

NTNU

Norwegian University of
Science and Technology

UNIVERSITY
OF OSLO